Technical University of Crete

School of Production Engineering and Management

Computational Mechanics and Optimization Lab (Co.Mec.O.)

Sheet Metal Forming simulation and Springback prediction based on Finite Element Analysis

Diploma Thesis by

Stefanos Christos Spathopoulos

Supervisor: Prof. Georgios E. Stavroulakis

Submitted in partial fulfillment of the requirements of Technical University of Crete for the Diploma of Production and Management Engineer.

Chania, October 2019

This page was intentionally left blank

Abstract

Sheet metal forming is one of the most important manufacturing processes applying in many industrial sectors with the most prevalent, automotive industry. The main purpose of that operation is to achieve the production of a desired formed shape blank, without causing any material failures. The specimen should as well conforms to the appropriate dimensions and tolerances, after reaching the unloading state. Over time, the automotive industry is constantly investing in material optimization, aiming at achieving a high-strength and reduced mass combination. As such, materials become increasingly complex, since their microstructure changes, which results in non-linear properties as well as complicated behaviors. Consequently, by aiming to improve the predictability, accuracy, and quality of a study, finite element software is frequently used in such processes. These simulation tools, conduct manufacturing operations analysis and after their results are elicited, they are cross-checked with experimental tests and thereby extract precise conclusions concerning materials behavior. During this thesis, the sheet metal forming simulation of an experimental automotive specimen as well as its spring-back prediction will be implemented by the finite element method. Initially, the related geometry, as well as its corresponding forming tools, will be designed through CAD software and then they will be imported in a simulation software through which an FEA analysis will be applied.

Περίληψη

«Προσομόιωση παραμόρφωσης μετάλλου και πρόβλεψη ελαστικής αποφόρτισης με χρήση πεπερασμένων στοιχείων»

Η παραμόρφωση μετάλλου αποτελεί ένα από τα σημαντικότερα είδη κατεργασιών και βρίσκει εφαρμογή σε πολλούς βιομηχανικούς κλάδους με έναν από τους πιο διαδεδομένους την αυτοκινητοβιομηχανία. Κύριος στόχος της αποτελεί η διαμόρφωση ενός μεταλλικού ελάσματος σε επιθυμητή γεωμετρία χωρίς την πρόκληση αστοχιών υλικού, όπως και η συμμόρφωσή του με τις ήδη μελετημένες διαστάσεις και ανοχές αφού αποφορτιστεί. Με την πάροδο του χρόνου ο κλάδος της αυτοκινητοβιομηχανίας επενδύει συνεχώς στην βελτιστοποίηση των υλικών που χρησιμοποιεί, θέλοντας να επιτύχει συνδυασμό υψηλής αντοχής ενώ παράλληλα και μειωμένης μάζας. Έτσι τα υλικά γίνονται όλο και πιο σύνθετα, ενώ μεταβάλλεται η μικροδομή τους, έχοντας ως αποτέλεσμα να εμφανίζουν μη γραμμικές ιδιότητες όπως και αρκετά περίπλοκες συμπεριφορές κατά την επεξεργασία τους. Συνεπώς με απώτερο σκοπό την βελτίωση της προβλεψιμότητας, της ακρίβειας όπως και της ποιότητας μιας μελέτης, χρησιμοποιούνται λογισμικά πεπερασμένων στοιχείων για τέτοιου είδους εφαρμογές. Αυτά τα εργαλεία προσομοιώσεων εκτελούν αναλύσεις των συγκεκριμένων διαδικασιών παραγωγής, ενώ στην συνέχεια τα αποτελέσματά τους εμφανίζονται σε εικονικό περιβάλλον και διασταυρώνονται με αυτά των πειραματικών δοκιμών, εξάγοντας με αυτόν τον τρόπο όσο το δυνατόν πιο ακριβή συμπεράσματα σχετικά με την συμπεριφορά των υλικών. Στην συγκεκριμένη εργασία θα προσομοιωθεί η διαδικασία κατασκευής ενός πειραματικού νεύρου που χρησιμοποιείται στην αυτοκινητοβιομηχανία, όπως και θα προβλεφθεί η ελαστική επαναφορά κατά την αποφόρτισή του μέσω της μεθόδου πεπερασμένων στοιχείων. Αρχικά θα μοντελοποιηθεί η κατάλληλη γεωμετρία όπως και τα αντίστοιχα καλούπια διαμόρφωσης, μέσω λογισμικού CAD, ενώ στη συνέχεια τα συγκεκριμένα μοντέλα θα περαστούν σε λογισμικό προσομοίωσης FEA οπού και θα εφαρμοστεί σχετική ανάλυση.

Acknowledgements

I would like to thank my supervisor, Prof. Georgios E. Stavroulakis for the opportunity he has given to me, as well as for his confidence during that thesis preparation.

I would also like to express my sincere gratitude to my family and friends, that stand by me and support me during that period of my life.

Special thanks to the people who along the way believed in me.

Contents

List of Tables

List of Figures

Chapter 1

Introduction

Sheet metal forming is widely used in many applications mainly in the automotive and aerospace industry. It is a very popular manufacturing technique due to the high precision, mass production and short processing time that can be provided in a production line. During recent years in automotive concepts, there is a high demand for light-weight car bodies including fuel efficiency, aiming to reduce CO2 gas emissions and generally environmental burden. Due to that, sheet metals such as high strength steels and aluminum alloys are becoming more important in the automotive industry but at the same time, they require innovative simulation techniques, in the design and development phase, as well as suitable processing chains. Some major negative consequences of those materials occur due to their high strength values, such as low formability and springback during unloading. Springback is a phenomenon with high importance in forming applications where dimensional precision is a vital requirement since the final product has to conform with the predefined engineering tolerances. During the unloading of the manufactured part, the strains of the material change and as a result, the final component dimensions are different than expected. Thus, the main target of finite element simulations is to closely investigate and minimize that issue, by replacing the physical tryouts from the virtual ones and improving the quality of the die design manufacturing cycle. That's why FEA has been already integrated into plenty of industrial applications [1],[2]

1.1 Scope and objective

The production of new parts in metal forming industry becomes more and more complicated, as time goes by. As a consequence, the manufacturing processes are also getting way more demanding, since many complex and small tolerances are requested. Therefore, finite element software provides the capability of building realistic simulation models, which contain complicated forming processes and are also capable of adapting to any corresponding needs. Hence, several solution methods have been developed, having a constant target of achieving the appropriate accuracy and computational efficiency of a model, since both of them really essential requirements for an FEA simulation. The primary objective of this study is to simulate the sheet metal forming procedure as well as the springback effect, on an S-Rail geometry. The simulation will be solved, using Explicit and Implicit methods, for the forming and the springback state respectively. Consequently, the elicited results will be compared with the outputs of an already published study, as well as the percentage error between them will be calculated. Last but not least, a springback sensitivity of the model will be conducted, by modifying some parameters of the simulation and then make comparisons between the elicited results.

1.2 Outline

This thesis will be organized as follows. In **Chapter 2**, an overview of the metal forming theoretical background is given, by describing some different forming techniques. Subsequently, the properties of a material, its actual behavior as well as the possible failures that can occur during sheet metal forming process, are indicated. **Chapter 3** deals with Finite Element Analysis, while it initially gives a theoretical overview concerning the solving techniques, element and contact types that can be utilized during a simulation. Afterward, it focuses on the methodology, as well as on the corresponding setup steps which are followed to model a finite element analysis. In **Chapter 4**, we evaluate the elicited results of the analysis after using two different materials, AL6111-T4 and HSS, as well as by modifying some of the simulation parameters, we investigate the springback sensitivity. In **Chapter 5** the thesis conclusions are drawn.

Chapter 2

Theoretical Background

In this chapter, a quick overview of the metal forming theoretical background will be given, by describing different forming processes. Subsequently, the properties of a material, its actual behavior as well as the possible failures that can occur during sheet metal forming process, will be indicated.

2.1 Sheet Forming processes

In modern industries, there are plenty of manufacturing processes applied in different sectors as well as for different applications. The two most commonly used procedures are, bulk metal forming and sheet metal forming. Bulk-Metal forming is the shaping of bodies with concentrated mass, which also have the same size and dimensions in all three orthogonal directions x, y, and z. On the other hand, sheet-metal forming is a forming process during which bodies with large initial extensions in two directions and small extension in the third one, such as a piece of sheet metal or steel plates, are deformed. Thus, as one can see, there are a few differences between those two manufacturing forming processes. By looking into more detail, during sheet metal forming a wide and thin blank is formed against a die, something that makes it impossible for the workpiece to be kept inside a closed dies configuration. The material in sheet metal forming is most commonly subjected to tensile stresses, whereas in bulk-metal forming compressive

stresses are dominating. Due to the existence of tensile stresses in sheet-metal forming, strong limitations occur from the aspect of possible workpiece shaping. As a consequence, during that specific procedure due to tensile and compressive stresses as well, some failures such as necking, buckling, and wrinkling could appear. [3] However, sheet metal forming is widely used in the manufacturing industry for plenty of applications as well as is divided into many subcategories, which are mentioned below:

Stretching

During that forming process, spherical shell products including singly curved or even doubly curved shapes can be manufactured, see Figure 2.1. At first, before the procedure starts, the sheet metal should be clamped. During the forming operation though, the punch is forced into the blank so as to deform the sheet metal over the punch face and in parallel to reproduce the die shape on the specimen. Through that process, similar products like in bending could be produced. However, since a higher amount of tension exists inside the blank during that method, one can observe greater thinning of the metal specimen. Apparently, due to those tensile stresses, the springback effect is significantly reduced compared to bending procedures. That kind of manufacturing process is extensively used when there is a need for strict geometrical tolerances for the final product.[3]

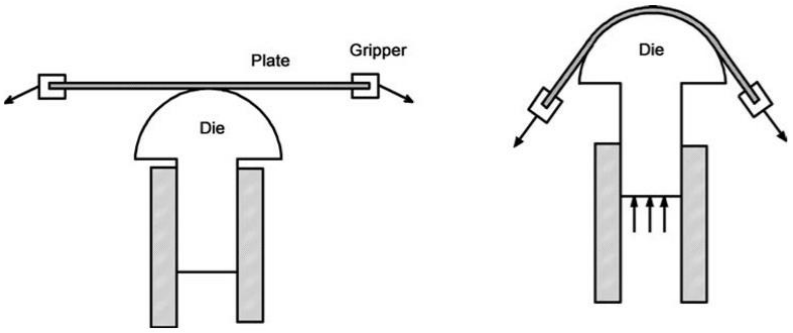

Figure 2.1 Sheet metal forming by stretch forming. **[3]**

Deep Drawing

A large number of parts used in everyday life are produced through that forming process, such as loaf pans and kitchen sinks. That procedure is implemented, by forcing a circular or rectangular upper punch with rounded corners down into a sheet-metal blank. In the meantime, the specimen is supported by the die and the upper blankholder at its circumference, under controlled pressure. The bottom die is hollowed at the center which is slightly bigger than the shape to be formed, see Figure 2.2. During that process, it is very important to maintain the appropriate contact pressure between the blankholder and the bottom die, in order not to provoke any failures to the specimen. Such failures could be the fracture of the bottom cup wall or wrinkling at the wall of the product, while applying too much or lower than appropriate pressure, respectively.[3]

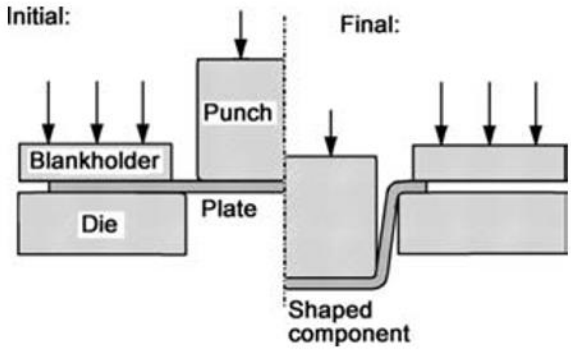

Figure 2.2 Deep drawing procedure. **[3]**

Bending

Bending is one of the most common methods used to change the shape of sheet metal with the simplest example of that process, the straight-line bending, see Figure 2.3. During that procedure, plastic deformation occurs only in the bend region while the material away from that area in not deformed at all. In case the material is not ductile, failures such as cracking may appear on the outside surface. Hence, something quite challenging during that process is to obtain an accurate and repeatable bending angle. [4]

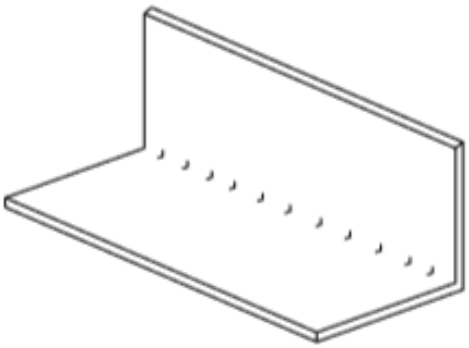

Figure 2.3 Straight Line bending [4]

There are various types of straight-line bending. In folding the workpiece is held steady on the one side and on the other one the edge gripes between the movable tools that rotate, Figure 2.4(a). In press brake forming the punch moves downwards and forces the sheet into a vee-die, Figure 2.4(b). Through roll forming, bends are being done continuously in roll strip, while in the corresponding machines a number of roll sets exist which are partially bending the sheet and thus wide panels such as roofing sheet or complicated channel sections can be easily manufactured Figure 2.4(c). Finally, flanging or wiping is another technique during which a stamped part accommodates a bending on its edge Figure 2.4(d). The workpiece is clamped on the one side and the flanging tool is moving downwards to bend the sheet.[4]

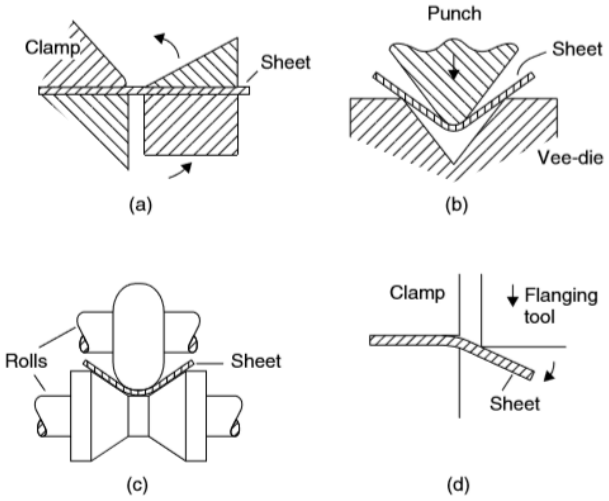

Figure 2.4 (a) Bending a sheet in a folding machine. (b) Press brake bending in a vee-die. (c) Section of a set of rolls in a roll former. (d) Wiping down a flange. [4]

Now in case the bending is not implemented along a straight line, or the blank is not flat, the plastic deformation is not only applying at the bent area but also in the adjoining sheet, see Figure 2.5(a). This could happen during shrink or stretch flanging. During shrink flanging, the edge of the workpiece is shortened and the flange may buckle, see Figure 2.5(b). Now during stretch flanging, the edge length must be increased and therefore splitting may appear, see Figure 2.5(c). [4]

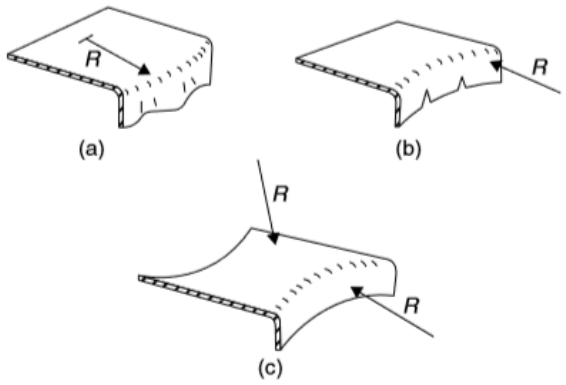

Figure 2.5 (a) A shrink flange showing possible buckling. (b) A stretch flange with edge cracking. (c) Flanging a curved sheet [4]

Stamping

Stamping operations convert coils of steel, received from the steel mill, into products. The whole stamping configuration consists of a punch, a draw ring, and a blank-holder, see Figure 2.6. The principles are more or less the same with stretch forming but the outer edge or flange is allowed to draw inwards under restraint to supply material for the part shape. Through that process, a large number of products are being formed and used in various applications, such as auto body panels. In most cases, those parts after being deformed, are assembled with other contextual products by welding, bonding or mechanical fastening. Usually, by that forming process, the really high production rate can be achieved since the tooling is well designed to produce vast quantities of parts with good dimensional control. The design of the forming tools requires a good combination of skills and powerful computer-aided engineering systems. However, for making conceptual designs and while trying to solve some issues, the complicated forming procedure can be broken down into basic elements and be simplified. [4]

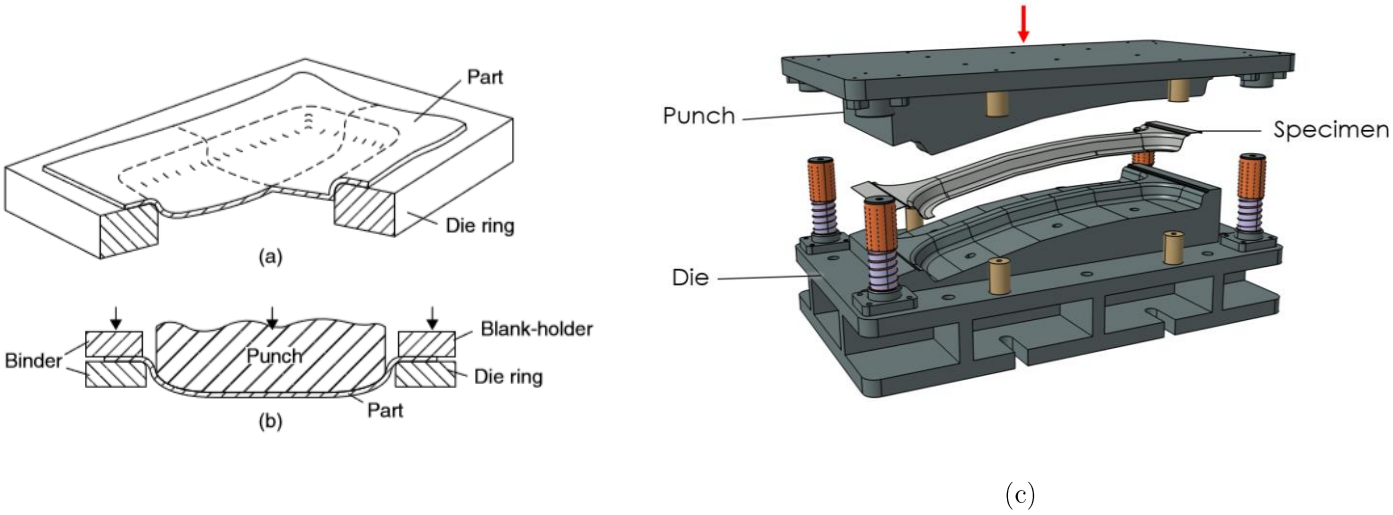

Figure 2.6 (a) Typical part formed in stamping or draw die showing the die ring, but not the punch or blankholder. [4] (b) Section of tooling in a draw die showing the punch and binder assembly. [4] (c) B-Pillar manufacturing configuration (Designed by S. Spathopoulos)

2.2 Different High-Velocity Forming processes

High-Velocity forming contains all processes converting stored energy in a really short time to plastic deformation. It can also be called impulse forming, high-energy-rate forming or high-strain-rate forming. That general process could be subdivided into high-velocity hydroforming, high-velocity mechanical forming and energy-based high-velocity forming, see Figure 2.7. The strain rates of that process are within the range of 10^2 to 10^4 s^{-1} or as well as into microseconds or milliseconds. Thus, the cycle times can vary depending not only on the handling operations duration but also on the process preparation, which some times can be complex and time-consuming. High-velocity forming has some great advantages. Some of those are firstly, the increased formability of the metal which can be achieved in several material types due to high strain rates (hyper-plasticity), the reduction of wrinkling and spring-back of the specimen, and last but not least the possibility of using inertia locking mechanisms in tool design which allows smaller-capacity presses to be utilized.[5]

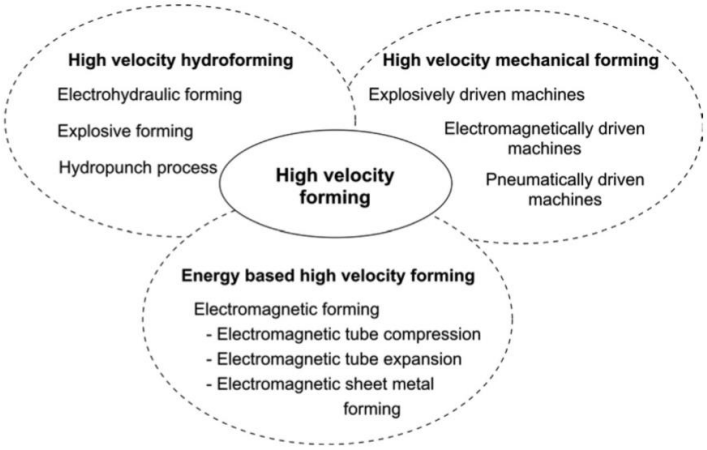

Figure 2.7 Classification of high-velocity forming technologies. [5]

High-Velocity Hydroforming

That specific process could be used in many different forming methods, such as deep drawing, stretch forming i.e., and the only forming tool required is a die since the punch force is applied through a medium (solid, fluid or gas). During that process, the pressure applied through the medium is not distributed in a continuous way uniformly. Actually, the pressure impulse propagates through it with a velocity higher than sonic speed, which is called shock wave. When that wave impulse hits the specimen, a part of the mechanical energy is transferred to the workpiece and accomplish the forming procedure. The forming range of the specimen depends on the pressure and pressure pulse duration which is translated into the velocity of the process. Due to the fact that the blank moves really fast, the tension from the shock wave that strikes on it perpendicularly usually produces cavitation behind the specimen. From that shock wave method, the two processes we are interested in, are electrohydraulic forming and explosive forming.

As for the **electrohydraulic forming**, the configuration consists of a capacitor that stores electric energy as well as from a spark gap that is suddenly discharged. That energy provokes ionization and vaporization of the fluid, which releases a shock wave and leads to specimen deformation. During that process, electric energy is directly transformed into mechanical. That method can be implemented with two setups, having different discharge process. In the first one, the capacitor is discharged through a wire, while in the second through a gap, see Figure 2.8.

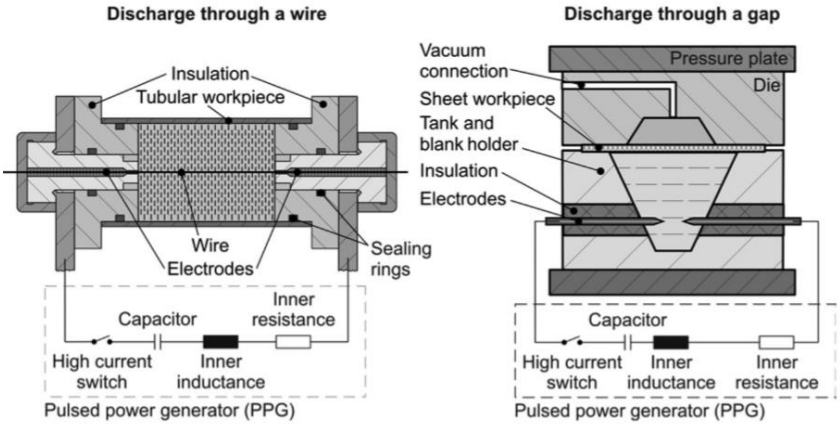

Figure 2.8 Different setups used in electrohydraulic forming according to German patent DE 1806283. [5]

That operation finds applications in automotive and aerospace sectors as well as air-conditioning technologies. Through that method, complex parts with small corner radii and reduced spring-back effects can be manufactured. Apart from that, due to the loading of the shock wave, wrinkling is prevented during conical pieces drawing. One can observe some examples of manufactured products in Figure 2.9.

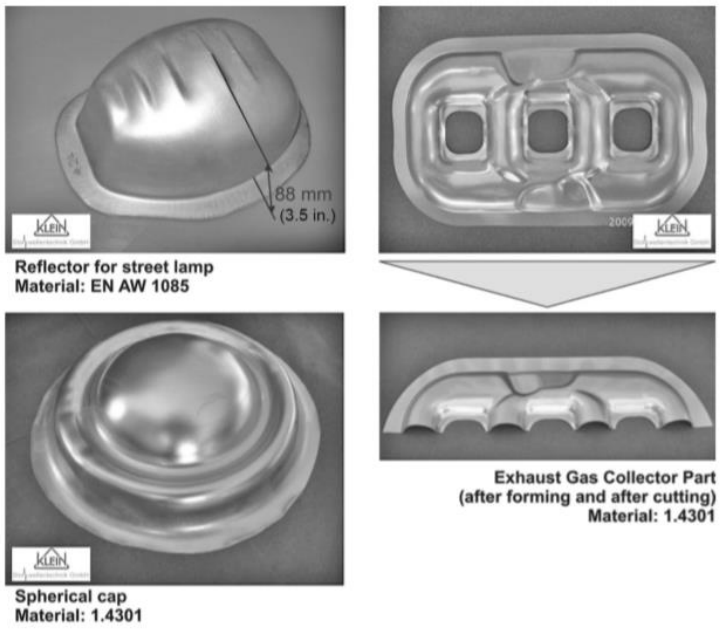

Figure 2.9 Parts produced by electrohydraulic forming [5]

Now as for the second process, **explosive forming**, the shock wave can be initiated not only through the detonation of high explosives but also propellant forming techniques

such as gas forming. There are two techniques that could be followed during that process, content operation and standoff operation. During the first case, one of the two workpiece surfaces is covered with the explosive while the detonation wave velocity reaches the workpiece in microseconds with very high speed. That process is usually applied when high pressure is required but is rather unprecise which keeps it limited to thick plates forming. Now as for the second, standoff operation, the die and workpiece are submerged into, preferably, fluid or amorphous substance and the explosive is kept in some distance from the specimen, see Figure 2.10. In fact, during that process, the shock wave is transferred through the fluid, and deforms the workpiece, while in parallel a gas bubble is produced, expanding in lower velocity than the wave, and hence deforms the workpiece once more. The pressure created during the process is significantly lower than the contact operation, while it increases proportionally to the distance between the explosive and the workpiece.

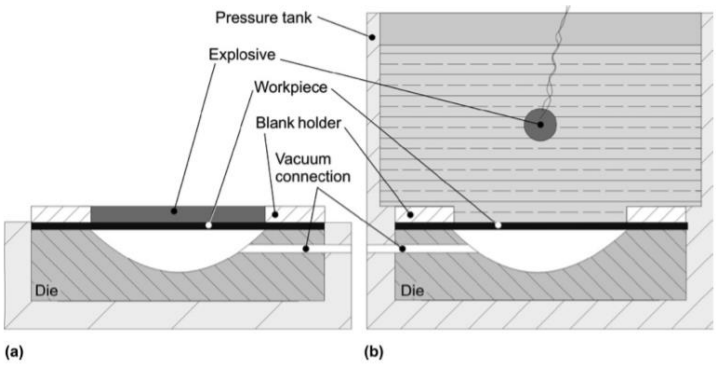

Figure 2.10 Process variations of explosive forming techniques. (a) Contact operation. (b) Standoff operation **[5]**

That process can be used in various applications and is suitable to form parts with quite complex geometries as well as materials with rather difficult formability under conventional methods. The sheet thicknesses which can be accommodated by that method are plenty and vary. The technologies applied to steel and aluminum are different as well as for high-strength titanium alloys. Thereby, such a forming process is suitable for large parts which cannot be manufactured with conventional methods, due to the insufficient forces of conventional presses. [5]

High-Velocity Mechanical Forming

During that process, presses with special systems which can provide relatively high velocities up to 20 m/s, are commonly utilized. Since these operations are considered to be essentially adiabatic, due to overcompensation of the temperature, there is some loss by the heat generated through forming. In general, the forming operation is performed in higher temperatures than the conventional process. Due to the high impact forces created, the life of the tools is relatively short as well as the cycle times are low. Hence, this type of method has been limited. The large variety of machines used for high-velocity mechanical forming can be subdivided into pneumatically-driven machines, explosively-driven machines, and electromagnetically-driven machines. From all those referred, only the third machine type still exists. [5]

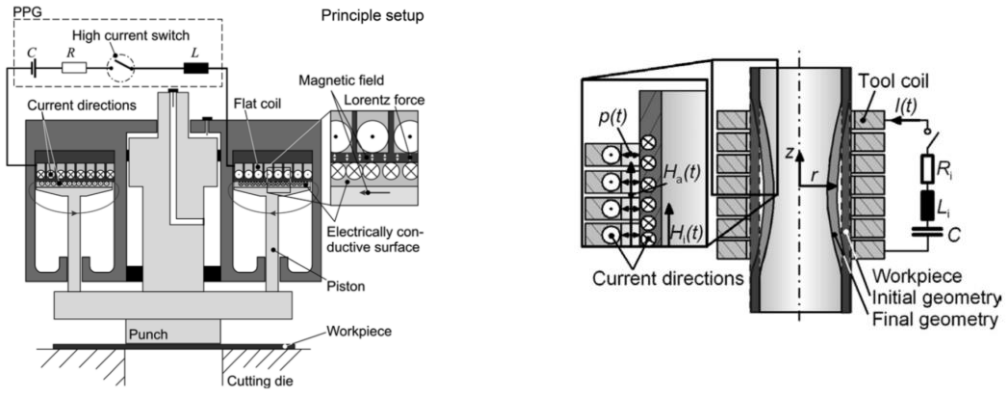

(a) (b)

Figure 2.11 (a) Principle of an electromagnetically-driven blanking press (b) Principle of the electromagnetic compression process **[5]**

Energy-based High-Velocity Forming

The main manufacturing method which represents energy-based forming procedures is **electromagnetic forming**. During that process, the sheet metal specimen is deformed through forces applied with pulsed magnetic fields, see Figure 2.12. That forming type has many advantages, a few of which are mentioned below. First of all, since the magnetic field represents an active tool, there is no need for medium in-between, and the

forces are applied to the workpiece without mechanical contact. Thus, the process should be performed under special conditions (in a cleanroom or vacuum) where the surface of the workpiece will not be affected by external factors. Apart from that, obviously that process is environmentally friendly since no lubricant is used, as well as no impurities involved. This results in no need to clean the workpiece after the procedure is finished. Subsequently, the ability to adjust forces through charging energy and voltage provides high repeatability of the process without damaging even the brittle metals. The applied forces magnitude, of course, depend on the formed material. Comparing to conventional sheet metal forming, due to the fact that EMF uses only one forming-tool only the die, there is a significant decrease in overall cost. Finally, something also important is the fact that in several materials having high strain rates, higher formability achieved comparing to conventional quasi-static operations. On the other hand, EMF, of course, has some disadvantages. To start with, due to the physics of this process, this technology works only with high-conductive materials while it gets more effective, by increasing conductivity and decreasing flow stress. In case the specimen conductivity is not enough, there is a possibility of using the so-called drivers. However, before one proceeds in such a way, it should be kept in mind that the cost will be increased as well as the handling and positioning will be more difficult. Apart from the already mentioned, due to high currents, high voltages and high magnetic fields, some safety aspects of the process and the equipment should be considered. [5]

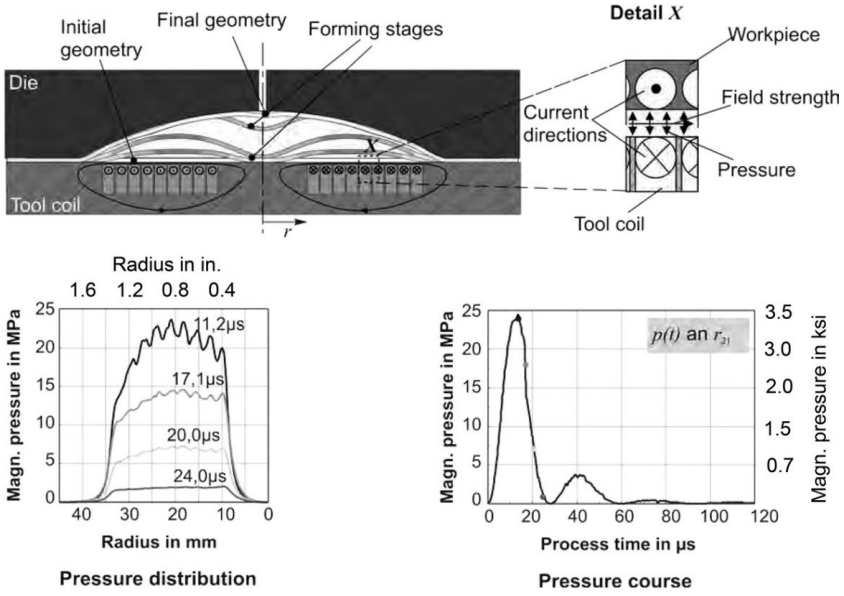

Figure 2.12 Principle of the electromagnetic process during sheet metal forming. [5]

2.3 Material Properties

Tensile test

Due to the easy performance, as well as for historical reasons, many familiar material properties are based on measurements made through the tensile test. A typical shaped piece, see Figure 2.13, is commonly used for that test which has initial dimensions of the length l_0, width w_0 and thickness t_0. A dragging force P is applied to the specimen and by using an extensometer it measures the change in length $\Delta l = l - l_0$. Sometimes a transverse extensometer is used as well in order to measure the change in width $\Delta w = w - w_0$. During that test, load and extension will be recorded and after those values are analyzed material properties diagrams will be created. [4]

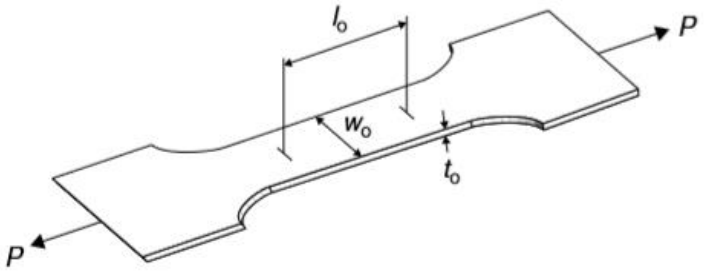

Figure 2.13 Tensile test strip [4]

Load-extension diagram

The relationship between the load and extension values, mentioned above, are plotted in the load extension diagram, see Figure 2.14. At the starting point, the extension is elastic but that specific part of the diagram is so small that it cannot be easily seen. This diagram gives some important information concerning the response of the material to a particular process and more specifically is the extension of a tensile strip with given width and thickness. One of the features extracted from that diagram is the *initial yielding load* P_y, during which plastic deformation begins. After that initial yielding point, a region consists of uniform deformation and increasing load, follows. This occurs due to *strain-hardening*. It is actually a phenomenon that appears in most metal alloys during

the soft condition, through which the strength or hardness of the material increases with plastic deformation. During the whole process, the cross-sectional area of the strip decreases as the length increases. When the strain-hardening effect is balanced by the rate of area decrease, the load reaches a maximum P_{max} and an actual point is reached. After that point, uniformity of deformation ceases, a diffuse neck develops in the smaller section of the specimen and it still continues until the piece fails. [4]

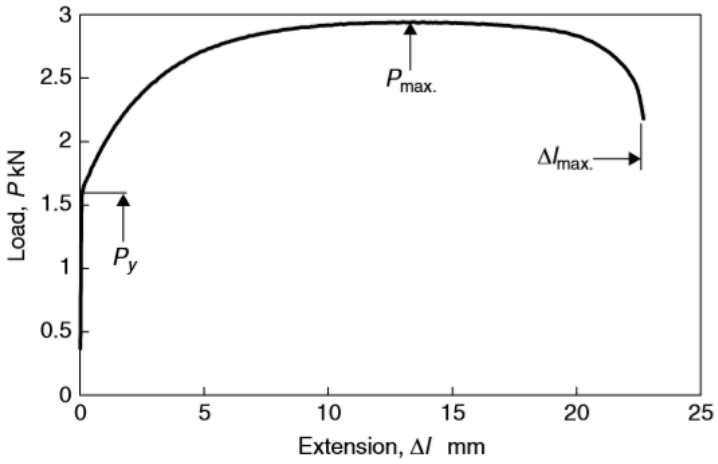

Figure 2.14 Load extension diagram for a tensile test [4]

At that specific failure point, the extension is Δl_{max} and the total elongation of the specimen can be defined by,

$$E_{T_0} = \frac{l_{max} - l_0}{l_0} \text{ x } 100\% \tag{2.1}$$

True stress-strain curve

Before starting the development of modern data processing systems, in order to obtain the *engineering stress-strain* curve, usually, the load is divided by the initial cross-sectional area, $A_0 = w_0 t_0$ and the extension by l_0. Although that type of curve is widely used, there are two drawbacks that affect the reliability of its results. First of all, the cross-sectional area decreases during the test, and consequently, the stress is

underestimated and second, the engineering is not a satisfactory strain measure because it is actually based on the original gauge length. In order to overcome these disadvantages, the forming processes studies are based on the *true stress-strain* curve. Those values can be calculated as follows:

$$\sigma = \frac{P}{A} \tag{2.2}$$

where A is the current cross-sectional area. *True stress* can be calculated form *load-extension diagram* during the rising part of the curve, between initial yielding and maximum load, by keeping in mind that plastic deformation occurs while volume change constantly as follows,

$$A_0 l_0 = Al \tag{2.3}$$

and the true stress is

$$\sigma = \frac{P}{A_0}\frac{l}{l_0} \tag{2.4}$$

If during a piece deformation, the gauge length is increased by a small amount of dl the *strain increment* or the extension of per unit current length, i.e.

$$\mathrm{d}\varepsilon = \frac{\mathrm{d}l}{l} \tag{2.5}$$

In case of very small length extensions, where $l \sim l_0$ the strain increment is nearly similar to the engineering strain but for larger strains, there is a significant difference. If the straining process continues uniformly in one direction, the strain increment can be integrated to give the true strain, i.e.

$$\varepsilon = \int d\varepsilon = \int_{l_0}^{l} \frac{dl}{l} = ln\frac{l}{l_0} \tag{2.6}$$

The true stress-strain curve calculated from the load-extension diagram is shown below in Figure 2.15.

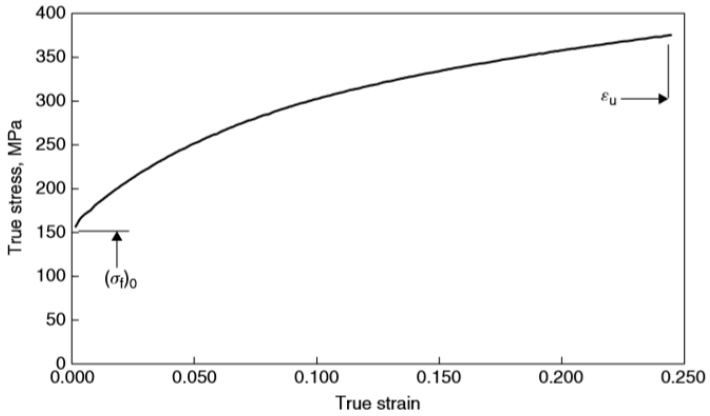

Figure 2.15 True stress-strain curve calculated from the load-extension diagram [4]

A common way to approximately define this curve is to use the simple power law

$$\sigma = K\varepsilon^n \tag{2.7}$$

where the exponent n is known as strain hardening index and K is the strength coefficient. That empirical equation known as *power-law* or *Hollomon's law*, see Figure 2.16 (a), is commonly used to describe the plastic properties of annealed low carbon steel sheet. Those material properties will be accurate, except for the small elastic part at the beginning of the curve. [4],[6]

An alternative commonly used law, known as *Swift's law* given by

$$\sigma = K(\varepsilon_0 + \varepsilon^n) \tag{2.8}$$

where ε_0 is called pre-strain or offset strain, see Figure 2.16 (b). This law will fit material with specific yield stress. If the material has been hardened in any previous process, this constant ε_0 indicates a shift in the strain axis corresponding to this amount of strain [6].

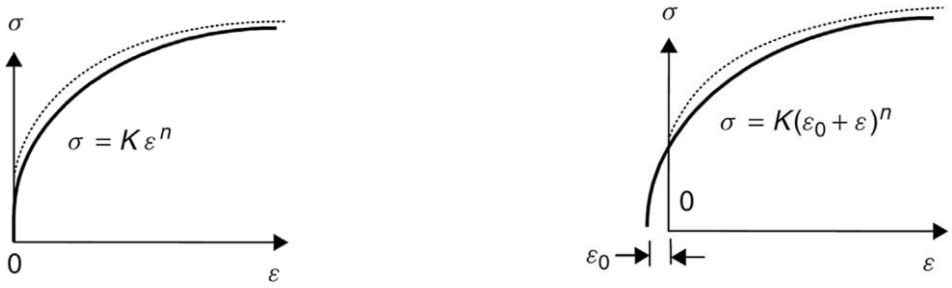

(a) (b)

Figure 2.16 Empirical stress-strain laws fitted to an experimental curve, (a) Power-law, (b) Power-law with initial strain. **[6]**

Anisotropy

A material having the same properties in any direction is called *isotropic.* Usually, most industrial sheets show a difference in properties which depends on the direction that is oriented. This type of variation is known as *planar anisotropy.* Furthermore, a difference could exist between the average properties in the sheet plane and those in the through-thickness directions. During tensile tests of a material that has the same properties in all directions, there is an expectation of width and thickness strains to be equal. If they are different, some *anisotropy* exists. In material which properties depend on direction, the anisotropy state is expressed through *Lankford parameter* or *anisotropy coefficient,*

$$R = \frac{\varepsilon_w}{\varepsilon_t} \tag{2.9}$$

which is actually the ratio of width strain,

$$\varepsilon_w = \ln \frac{w}{w_0} \tag{2.10}$$

to thickness strain,

$$\varepsilon_t = \ln \frac{t}{t_0} \tag{2.11}$$

Frequently the thickness strain is measured directly, but there is a possibility to be calculated from length and width measurements, using constant volume assumption, i.e.

$$wtl = w_0 t_0 l_0 \tag{2.12}$$

or

$$\frac{t}{t_0} = \frac{w_0 l_0}{wl} \tag{2.13}$$

Consequently, the *anisotropy coefficient* is indicated as follows,

$$R = \frac{\ln \frac{w}{w_0}}{\ln \frac{w_0 l_0}{wl}} \tag{2.14}$$

In case the width change is measured during the test, R-value can be determined continuously and some strain variation may occur. The direction of the R-value measurement is indicated by R_0, R_{45} and R_{90} for rolling, diagonal and transverse testing respectively. In case these values are different, for a given material, the sheet is displaying *planar anisotropy* and often described with,

$$\Delta R = \frac{R_0 + R_{90} - 2R_{45}}{2} \tag{2.15}$$

which may be positive or negative but steels are usually positive. Now when the R-value is different from unity, there is a difference between average in-plane and through-thickness properties, something that is usually characterized by a *normal plastic anisotropy ratio*, defined as, [4]

$$\overline{R} = \frac{R_0 + 2R_{45} + R_{90}}{4} \tag{2.16}$$

Rate Sensitivity

On many material properties, the strain rate usually has effects that are neglected. However, if the speed of the punch v is increased, a small jump in the load may be observed, as in Figure 2.17. This shows that the material has *strain-rate sensitivity* which can be described by the exponent m in the following equation,

$$\sigma = K\varepsilon^n \dot{\varepsilon}^m \tag{2.17}$$

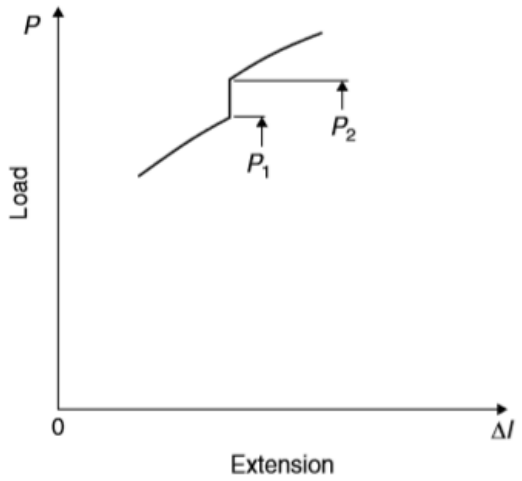

Figure 2.17 Part of a load-extension diagram showing the jump in load following a sudden increase in extension rate [4]

The strain rate is

$$\dot{\varepsilon} = \frac{v}{L} \tag{2.18}$$

where L indicates the length of the parallel reduced section of the specimen. The exponent m from the load and punch speed, before and after the speed change, denoted below, [4]

$$m = \frac{\log(P_1/P_2)}{\log\left(\frac{v_1}{v_2}\right)} \tag{2.19}$$

2.4 Material Behavior

Sheet deformation processes

We consider a workpiece Figure 2.18 with dimensions of length l, width w, and thickness t. Hence the principal directions are also denoted as 1 along the length, 2 across the width and 3 through the thickness of the workpiece. By applying a tensile force to the specimen, the part will deform in every dimension by dl, dw, dt which actually translated across the length, the width and the thickness respectively.

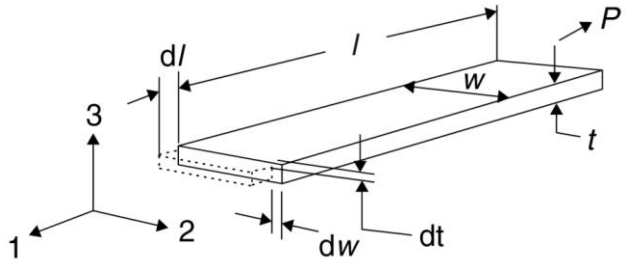

Figure 2.18 The tensile-test workpiece subjected to uniaxial deformation [4]

The principal strain increments are given by the following equations,

$$\mathrm{d}\varepsilon_1 = \frac{dl}{l}, \qquad \mathrm{d}\varepsilon_2 = \frac{dw}{l}, \qquad \mathrm{d}\varepsilon_3 = \frac{dt}{l} \tag{2.20}$$

It is well known that since during plastic deformation constant volume is maintained, strain increments keep the following relationship between them,

$$d(lwt) = d(l_0 w_0 t_0) = 0 \tag{2.21}$$

and we obtain

$$dl * wt + dw * lt + dt * lw = 0 \tag{2.22}$$

or, dividing by lwt,

$$\frac{dl}{l} + \frac{dw}{w} + \frac{dt}{t} = d\varepsilon_1 + d\varepsilon_2 + d\varepsilon_3 = 0 \tag{2.23}$$

That phenomenon is called the *incompressibility condition*.

In a typical sheet process, the workpiece deforms under non-zero membrane stresses σ_1 and σ_2 comparing to the tensile test, that we investigate above, in which they are both zero. The third stress σ_3 , perpendicular to the surface of the sheet is usually quite small and since we want to work on *plane stress deformation* we assume that is zero.

For such kind of sheet plane processes, the relations between principal stresses are the following

$$\sigma_1 \ , \quad \sigma_2 = a\sigma_1 \ , \quad \sigma_3 = 0 \tag{2.24}$$

and for strains,

$$\varepsilon_1 \ , \quad \varepsilon_2 = \beta\varepsilon_1 \ , \quad \varepsilon_3 = -(1+\beta)\varepsilon_1 \tag{2.25}$$

where α and β are the stress and strain ratios respectively. [7]

When external forces are subjected to a material body, it deforms. The way that body changes shape, depends on the magnitude of load applied as well as its material. The deformation types are elastic, viscoelastic and plastic. To start with, elastic is a reversible and time-independent deformation. Then viscoelastic which is a reversible but time-dependent deformation is increasing with time after load applies and starts decreasing slowly after the load removed. Finally, plastic in which the deformation stays permanent. Plasticity theories in general deal with stress-strain and load-deflection relationships for ductile material or structures that plastically deform.

Plasticity can be approached in two different ways. The first one is a mathematical theory which represents experimental observations as general mathematical formulations, based on assumptions and hypothesis of experimental results. The second one is a physical theory that focuses on the investigation of plastic deformation at the microscopic level while trying to explain how and why plastic deformation occurs. Concerning, the plasticity mechanics, one should investigate the microstructure of the material as well as its plastic flow and deformation mechanisms at the microscopic level, so as to be understood in a better way. [8] Some fundamental elements of plastic deformation are the following: Yield criteria, Material hardening, and Springback effect.

Yield Criteria

The yield surface is one of the most important concepts in material plasticity due to the fact that it separates the elastic from the plastic region. It actually defines the stress level beyond which plastic deformation occurs and also constitutes a very important element for the strains. A yield criterion is basically the critical point where the deformation state changes from elastic to plastic. The general formula which expresses the critical point in a mathematical way is the following:

$$F = 0 \tag{2.26}$$

while elastic deformation exists when the equation is,

$$F < 0 \tag{2.27}$$

The yielding criterion varies based on the corresponding material type. As mentioned during the previous chapter (2.3), **isotropic** is defined as the material whose properties are the same in every direction while contrariwise **anisotropic** materials properties differ with the orientation change.

In case the material studied is isotropic, yielding depends only on the principal stresses magnitudes and yield criterion is expressed as follows,

$$F(\sigma_1, \sigma_2, \sigma_3) = 0 \tag{2.28}$$

On the other hand, for a fully anisotropic material, the initial yield criterion in terms of principal stresses and principal directions $n_i \quad i = 1,2,3$ is expressed as follows,

$$F(\sigma_1, \sigma_2, \sigma_3, n_1, n_2, n_3) = 0 \tag{2.29}$$

The equation above points out that both the intensity of stress tensor (principal stresses) as well as its orientation (principal directions) are equally important for the anisotropy yielding. [8]

There are plenty of theories available for predicting yield conditions for both isotropic and anisotropic materials. However, during that thesis, we will delve into details only for the isotropic ones. Those theories are based on a different hypothesis about material behavior and results in yield functions of different forms. For isotropic material, plastic yielding depends only on the magnitude of the principal stresses and not on their directions. The most widely used isotropic yield models are *Tresca* and *von Mises* criterion. [6]

The first, as well as the oldest one, is the *Tresca yield criterion* on which yielding occurs when the greatest maximum shear stress reaches a critical value. During a tensile test where $\sigma_2 = \sigma_3 = 0$ the greatest maximum shear stress at yielding is $\tau_{crit.} = \sigma_Y/2$. Hence in theory yielding will occur in any process when

$$\frac{\sigma_{max.} - \sigma_{min.}}{2} = \frac{\sigma_Y}{2} \tag{2.30}$$

or

$$|\sigma_{max.} - \sigma_{min.}| = \sigma_Y \tag{2.31}$$

The *Tresca yield criterion* in-plane stress can be depicted graphically through the hexagon shown in Figure 2.19. The stress state at yield, as the stress ratio a change, is indicated by the locus point P which is actually the hexagon. In the case of work-hardening material, as σ_Y increases the locus expands proportionally while if only instantaneous conditions considered, the flow stress remains constant. [4]

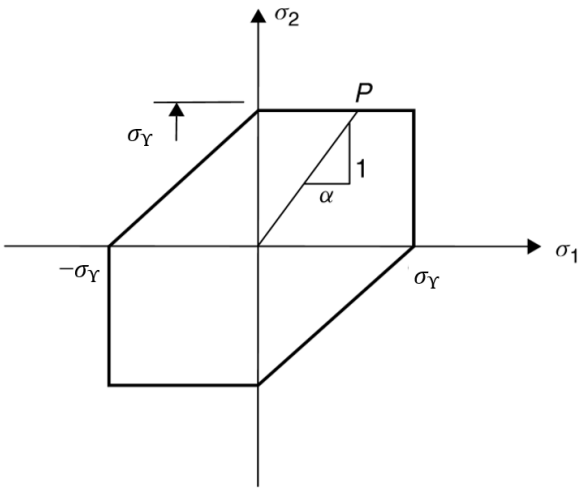

Figure 2.19 Tresca yield criterion locus.

The second theory is *von Mises yield criterion* which suggests yielding when the root-mean-square value of maximum shear stresses, reaches critical value, see Figure 2.20. During tensile stress at yield point, two of the maximum shear stresses will have the value of $\sigma_Y/2$ and the third one is equal to zero. Hence the criterion can be expressed as follows,

$$\sqrt{\frac{{\tau_1}^2 + {\tau_2}^2 + {\tau_3}^2}{3}} = \sqrt{\frac{2\,(\sigma_Y/2)^2}{3}} \tag{2.32}$$

or

$$\sqrt{2\,({\tau_1}^2 + {\tau_2}^2 + {\tau_3}^2)} = \sigma_Y \tag{2.33}$$

Substituting principal stresses for maximum shear stresses yielding condition can be expressed also as

$$\sigma_Y = \sqrt{\frac{1}{2}\{(\sigma_1 - \sigma_2)^2 + \ (\sigma_2 - \sigma_3)^2 + \ (\sigma_3 - \sigma_1)^2\}} \tag{2.34}$$

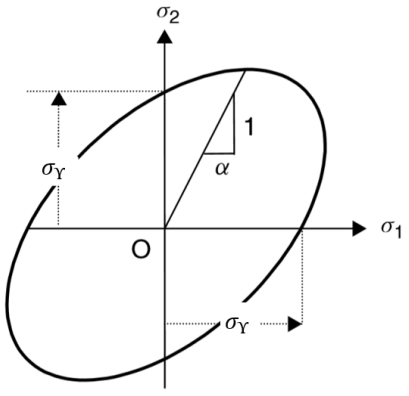

Figure 2.20 Von Mises yield criterion locus.

Both above theories apply only to isotropic material, being a reasonable approximation of experiments. Despite the fact that there are major differences in the mathematical

equations and methods that those criteria follow, the predicted stress values will normally not have a difference bigger than 15%. [4]

Now as for the anisotropic materials, since they are supposed to have anisotropy with three orthogonal symmetry planes, in order to be accurately modeled plenty of yield criteria have been developed by different research groups. Some of those are Hills criteria, Hershey 1954, Barlat and Lian 1989 criterion, the Cazacu-Barlat criterion (Cazacu and Barlat 2001), the Vegter criterion (Vegter et al. 1995), and the BBC (Banabic-Balan-Comsa) criteria (Banabic et al. 2000). Currently, the most frequently used are Hill 1948, Hill 1990, and Barlat 1989 (Banabic 2010).

Material Hardening

After yielding point, the materials are capable of resisting even further increase in load. This happens due to the hardening of the material. Many models can be used to model this effect and in the following section, some of the most commonly used in metal forming calculations are given. One of the rather essential choices is whether to model the material as isotropic hardening or kinematic hardening. In some cases, where the material deformation can be regarded as monotonic, it is not necessary to be that concerned about the hardening rule. However, in many cases, reversed deformation is present (this could be bending and subsequent unbending) and here it can be of major importance to include the correct type of hardening. [9]

To start with, regarding **isotropic hardening**, it's a process that can be considered when the material deformation is monotonous and proportional. Thus, the initial yield surface expands in all directions uniformly (Figure 2.21). Under this assumption, the yield surface can be expressed as follows

$$\sigma_Y = \sigma_{Y0} + H\varepsilon_{11}^p \tag{2.35}$$

where σ_Y denotes the current yield stress, σ_{Y0} the initial yield strength, H denotes plastic modulus, which is defined as the slope of the non-linear part of the stress-strain curve and ε_{11}^p is the plastic part of the normal strain ε_{11}. In fact, whether the material will show true hardening, perfect plasticity or softening behavior depends on the plastic

modulus value. If $H > 0$ the yield stress will increase, when $H = 0$ then it corresponds to perfect plasticity and in case $H < 0$, softening character is exhibited. [10]

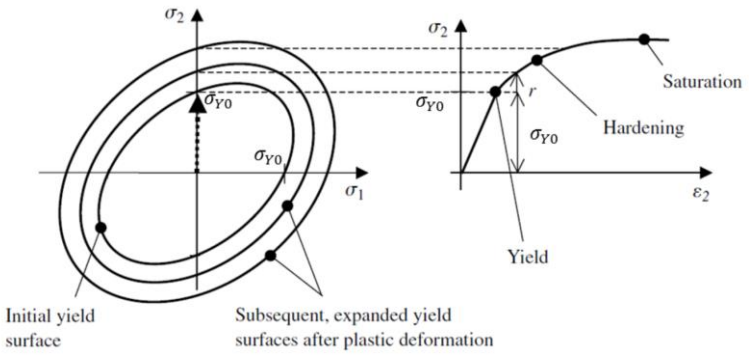

Figure 2.21 Isotropic Hardening: Left: Uniform expansion of the yield surface in stress space with plastic deformation. Right: Stress (σ) strain (ε) curve, representing an increase in the yield strength due to strain hardening [10]

When a material undergoes non-monotonic deformations, the isotropic kinematic model is not sufficient enough to describe its behavior. When the specimen removed from the tools and elastic unloading appears one can observe that yield strength during compression is much smaller than yield strength in tension. That phenomenon which occurs in metal plasticity is known as **kinematic hardening** or **Bauschinger effect**. In other words, one could say that yield surface without its shape and size be changed, it translates by moving into stress space and shifts to a value of α_{ij} i.e. the second-order tensor or back stress, see

$$f = f(\sigma_{ij}, \alpha_{ij}) = f(\sigma_{ij} - \alpha_{ij}) - \sigma_{Y0} \tag{2.36}$$

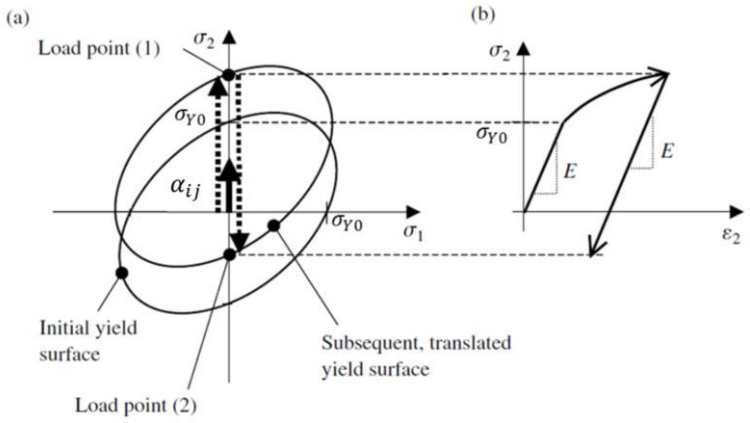

Figure 2.22 Bauschinger effect: (a) Schematic representation of the yield surface translation in stress space with plastic deformation. (b) Stress (σ) strain (ε) curve, representing different yield strength in the compressive regime and for monotonically increasing load [10]

Springback effect

Springback effect is considered as one of the most important issues in sheet metal forming. Therefore, many studies have been done, aiming to eliminate its presence in every deformation process. The main reason why it actually appears is the over-stress of the material beyond the yield strength in order to achieve the needed deformation. Upon unloading in a stamping process there is elastic recovery, during which stress returns to zero by following a path, parallel to the material elastic modulus, see in Figure 2.23. Thus, after releasing the forming load one can observe that permanent deformation is always less than expected and more accurately speaking spring-back is equal to the amount of elastic-strain recovered when the tool is removed, which usually causes major problems in the assembly. Due to that, FEA software not only contributes to forming procedures predictions but also, they deal with simulations of spring-back results. This is something absolutely mandatory and by using it at the model preparation stage, it enabled a far better tooling design as well as saved a considerable amount of testing time and financial cost.[11] Springback process is sensitive in many factors, such as material variations in mechanical properties, sheet thickness, tooling geometry, processing parameters, and lubricant condition.

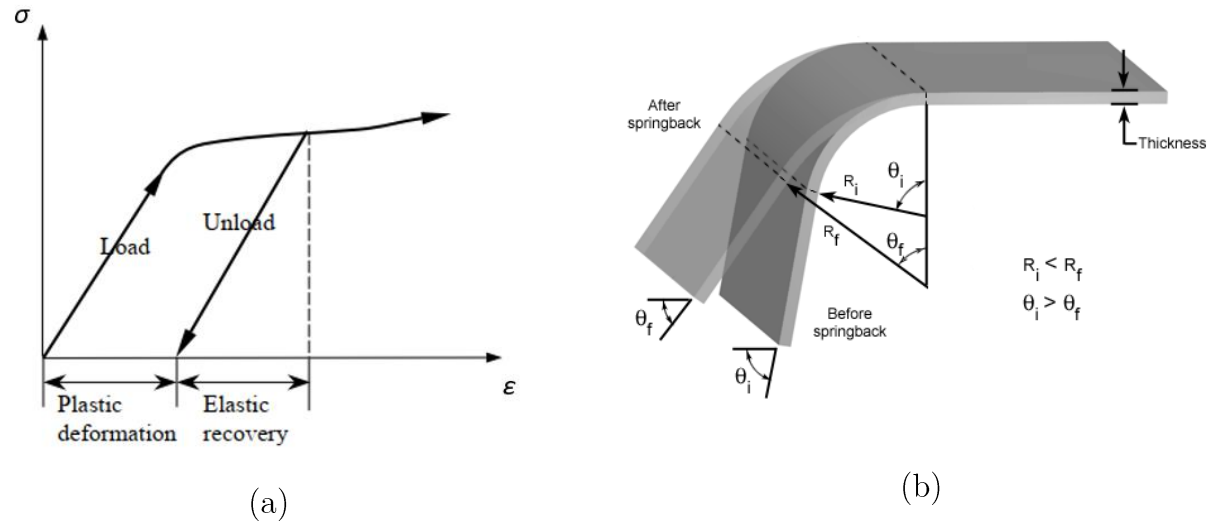

Figure 2.23 **(a)** Springback phenomenon **[8]** (b) Sheet metal before-after elastic unloading.

By looking into more detail, the whole process during unloading will be investigated. When a sheet is bent up to a particular curvature, at some point the bending moment is released and an unloading state starts, the elastic recovery causes the stress redistribution which is actually the springback. During that phenomenon, a change in curvature and bending angle occurs. The length of the mid-surface is

$$l = \rho\theta \tag{2.37}$$

This will not change during unloading since strain and stress in the middle surface are both zero. From this, we obtain

$$\theta = \frac{l}{\rho} \tag{2.38}$$

By differentiating the equation above (2.38) in which l = constant, we obtain

$$\frac{\Delta\theta}{\theta} = \frac{\Delta(1/\rho)}{1/\rho} \tag{2.39}$$

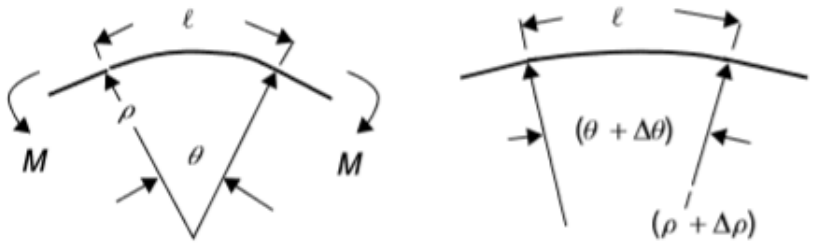

Figure 2.24 Unloading a sheet that has been bent by a moment without tension.[4]

2.5 Material Failures in SMF processes

Types of Failures

In sheet metal forming, the process may be terminated at a specific point by a number of events and the prediction of their limits is quite important. Each process has its own limiting events and although it is not easy to judge from first sight which one is the govern, it is usually one of the following, [7]

- Localized necking or tearing: At the starting point of tensile deformation, the process is stable as well as homogeneous over the specimen. When the forming process reaches a state in which a large number of strains localize in a small region of the workpiece, the local cross-sectional area starts to decrease which results in a local neck. In case the procedure continues, a great percentage of deformation will be concentrated on that necking, and since it is rather an unstable state will eventually lead to the tearing of the material. The main reason for facing that situation is the imperfections of nearly all real materials, such as small local variations in dimensions and composition, which usually lead to stresses and strains local fluctuations.

- Fracture: In failure analysis, one can segregate ductile and brittle failure. In fact, ductile is more or less common with tearing during localized necking in which material experience high deformation before failure. On the other hand, brittle fracture material is imperceptibly or even not deformed before fracture, which is characterized by rapid crack propagation.

- Wrinkling: It occurs when compressive principal stress exists inside an element and results in *buckling* or *wrinkling* of the workpiece. This is called *compressive instability* and resembles the buckling of a column.

Forming Limit Diagram (FLD)

The Forming Limit Diagram is a constructive concept which is used to characterize sheet metal formability. Since material selection, tools design and tryouts are really important for forming operations, it is considered as an essential tool for such processes. During sheet metal forming procedures, severe strain-path changes are a high influence for forming limits. Given that strain paths are not proportionally distributed, FLD is a really useful tool in the sense that it helps to understand material behavior under complex loading as well as contributes to the optimization of the die shape, aiming to avoid any kind of material failure [12].

The Forming Limit Curve (FLC) is a limit through which the maximum strain combinations that a metal blank can undergo are defined. That limit curve is constructed not only by implementing a biaxial stretch test via a hemispherical punch but also through a tension test to stretch the workpiece and simultaneously write down the major and

minor strains, ε_1 and ε_2 respectively, before any type of failure occurs. These types of strains can be measured through the use of grid circles near to a local neck of the deformed specimen. The procedure of measuring is implemented by marking a workpiece with an initial thickness t_0 with a grid of circles of diameter d_0 or a square mesh of height d_0 , as shown in Figure 2.25(a). Then during the uniform deformation, those marked circles will deform and obtain an elliptical shape of major and minor axes d_1 and d_2 respectively. Given that the square grid is aligned with the principal directions, it will become rectangular as shown in Figure 2.25(b).

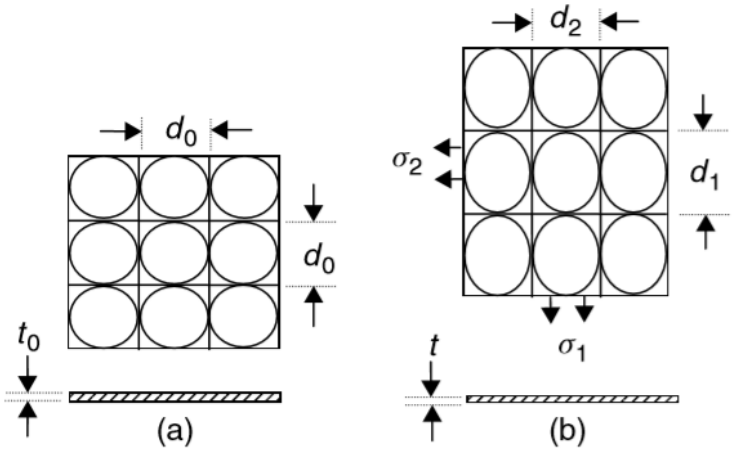

Figure 2.25 A sheet element in (a) undeformed state of an element with a circle and square grids marked (b) deformed state with the grid circles deformed to ellipses of major diameter *d1* and minor diameter *d2.* [4]

By measuring the strains of many different strain paths FLC can be defined, which is actually delineating the uniform straining boundary as well as the local necking onset. By the way, in practice, there is a scatter in the measured necking strains which actually means that one should consider a band rather than a single curve of those failures to occur.

One of the most important factors which affect the Forming Limit Curve (FLC) is the *strain-hardening* index n. The *n* changes proportionally with the height of the curve, so when the index decreases the height of the curve also decreases. During forming processes in which biaxial stretching is required to deform the workpiece, it is common for fully annealed metal to be used which means that the sheet material has high *n*. Unfortunately, materials with high *strain-hardening* index usually have low initial strength. One of the

strengthening processes that can reduce n and make forming much more difficult is cold-working. [7]

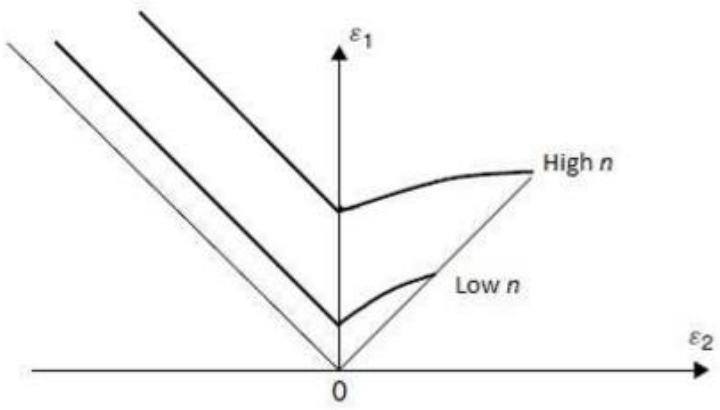

Figure 2.26 Difference of Forming Limit Curve (FLC) with high and low strain hardening exponent n. [7]

There are some other factors that are also affecting FLC, but not in the highest possible percent. First is *rate sensitivity* which although it doesn't affect the strain while tension reaches the maximum, influences the rate growth of a neck by delaying it. Apart from that, FLC is also affected by *ductile fracture, inhomogeneity,* and *anisotropy* but in a different way and percentage. [4]

The Forming Window

Sheet metal forming processes can be limited by various events such as local necking and tearing. Except for the already mentioned, something also possible to occur is a fracture of a ductile sheet at a necked region or before necking appears. Different limitations include sheet wrinkling under compressive loading. Something important to be mentioned is that sheet can only be deformed by tensile forces, so one of the principal stresses must be positive, or nearly zero. Considering all those factors, creating *a forming window* in which plane stress sheet forming is possible, seems to be really useful, see Figure 2.27. Note that the compressive limit where major tension reduces to zero is displayed at the strain path of $\beta = -2$. The wrinkling limit is only shown as a region in the second and fourth quadrants since is not completely a material property. That

diagram is only for visual help because it has been noticed that in case strain hardening index n, reaches a low value, forming window gets really narrow. In general, it is common for strengthening processes to reduce sheet strain-hardening. Hence one of the sheet metal forming challenges is to invent procedures that would be able to deform strong materials and simultaneously permit safe straining even though the narrow window. [4]

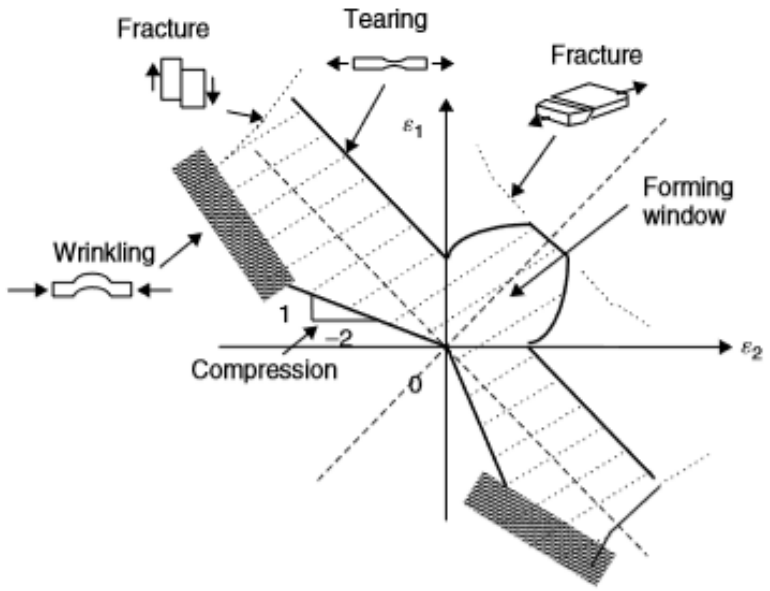

Figure 2.27 The forming window for plane stress forming of sheet [4]

Chapter 3

Finite Element Analysis

This chapter deals with FEA, while we will initially give a theoretical overview concerning the solving techniques, element and contact types that can be utilized during a simulation. Afterward, we will go through the procedure of preparing a sheet metal forming and springback simulation, as well as we will go into detail concerning the corresponding simulation setup steps that are followed.

3.1 Time Integration schemes

During the recent years, the Finite Element method is considered as a powerful analytical tool which can compute the solution of a continuum problem by reducing it to a system of an algebraic equation, [13]. By using that tool, combined with a powerful computer configuration, one can establish as well as solve governing equations for complex systems in a very effective way. The finite element method was initially developed in order to simulate problems in structural mechanics [14]. However, it was soon recognized that it can be equally applied in various types of engineering as well as in modeling of fabrication processes. When a fabrication process like sheet metal forming with high

deformation is being modeled, the evaluation of the stresses, strains, as well as the contact issues must be considered. One major advantage of FEA is the fact that it can be applied to a wide range of engineering problems and adapt to any corresponding needs. However, some basic requirements that an FEA engineer should keep in mind and follow while modeling a simulation are the following: simplicity, accuracy and computing efficiency. During sheet metal forming, finite element analysis software, contributes in the efficient design of the tooling. Thus, one can observe that is really cost and time effective than making real trial and error experiments. The main target of such software is to make predictions concerning the material behavior of a blank subjected to plastic deformation as well as the elastic unloading. Afterward, the forces, stresses, and strains should be evaluated and in parallel one should consider, whether is feasible for a simulated product to be manufactured in reality.

Methods

As mentioned above, during recent years, the finite element method (FEM), has gained much popularity in both the research and industrial sectors. In the meantime, several algorithms with various computational costs have been developed, providing different ways of simulation depending on the complication, the user needs as well as the problem nature itself, see Figure 3.1. Thus, in case one would like to solve a problem in the appropriate way, the advantages and disadvantages of those algorithms should be well understood.

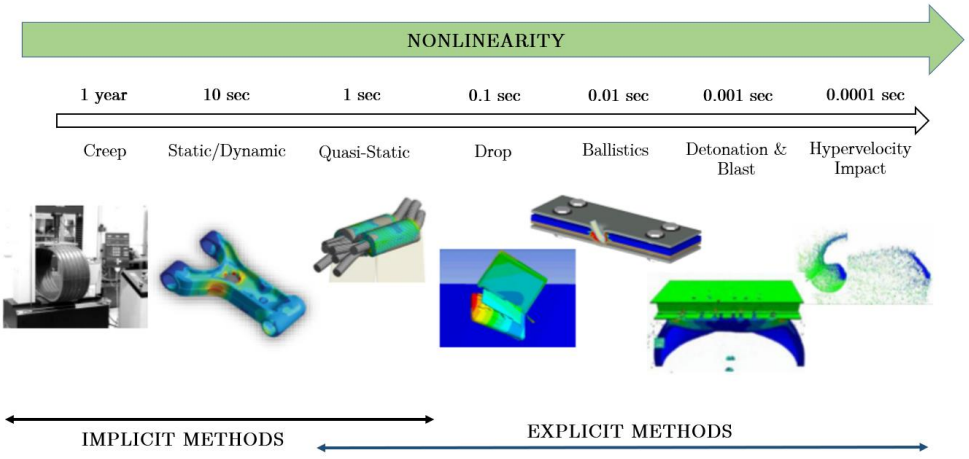

Figure 3.1 Problem time magnitude for Explicit and Implicit FEA methods

Implicit method uses an automatic incrementation strategy, to solve a large system of equations. It requires a lot of storage and CPU time but has certain advantages, something that, of course, depends on the type of analysis. One of the major advantages is the unconditional stability of that particular method. However, it can encounter some difficulties while trying to reach convergence on a complicated 3D model. As the reduction of the time increment continues, the computational cost in the tangent stiffness matrix is dramatically increased and causes divergence. Local instabilities cause force equilibrium to be difficult to be achieved.

Explicit method is frequently used, by aiming to overcome the implicit method difficulties and it has a great advantage of being easy and straightforward. Since external and internal forces difference, defines the nodal acceleration values at every time increment starting point, unbalanced forces don't exist and also there is no need to generate stiffness matrix. As long as those unbalanced forces do not exist, the explicit method is not facing any convergence problems. The main disadvantage is that it is stable under specific conditions as well as the maximum time increment is extremely small. That conditional stability means that time increment should be less than the critical value. That value can be approximated by the smallest time needed for an elastic wave to cross one element. Usually, the technique followed to solve that problem and decrease computational time is mass scaling. Through that method, the mass of material is artificially increased and also the critical time increment does. Although this type of method is basically meant to be used for short transient and dynamic problems, it can be also used for quasi-static but the inertia effects should be small enough to be neglected. Now as for the CPU cost, it depends on the size of the FEA model and how complicated is the model which is simulated. For instance, the implicit method is much more effective and faster in small problems but on the other hand, explicit is relatively better in the more complex ones which include larger and finer meshes.

In general, sheet metal forming as well as springback FEA simulations, have been investigated by various researchers. Therefore, we can conclude that both explicit and implicit methods can be used for such processes. The most commonly used, effective, as well as efficient procedure is to simulate the dynamic deformation of the blank through the explicit method and then use the implicit one for the elastic unloading. In case springback is simulated through the dynamic explicit scheme, dynamic oscillations will appear on the blank and as a consequence, the final static shape of the workpiece will not be

achieved. However, there is a possibility for those oscillations to be suppressed by using artificial damping but again the entire procedure remains pretty much inaccurate and unreliable. Hence, that combination of both Explicit & Implicit methods seems to be the optimal choice, since only the advantages of both schemes are kept and used efficiently by switching from one scheme to the other at the appropriate time point during the simulation. In particular, the dynamic explicit code is used only for the deformation phase in order to avoid implicit code's convergence problems and after the forming part finishes, the analysis changes to implicit method automatically in order to implement the spring-back process in a static way. [8],[15],[16],[17],[18]

In order to get into more detail regarding those two techniques, the mathematical background behind both Explicit and Implicit methods will be displayed

Mathematical approach

When working with a set of equations which depends on time, there is a need for making a time discretization of $0 = t_0 < t_1 < t_2 < \cdots < t_L = T$ with time steps $k_n = t_n - t_{n-1}$.

In sheet metal processes, there is the interest of solving the following equation

$$KU + C\dot{U} + M\ddot{U} = F \tag{3.1}$$

where $\boldsymbol{U}$ are displacements, $\boldsymbol{K}$ linear elastic forces, $\boldsymbol{C}$ damping forces, and $\boldsymbol{M}$ inertia forces.

By discretizing at time t_{n+1}, the equation (3.1) will be as follows

$$M\ddot{x}_{n+1} + C\dot{x}_{n+1} + f^{\mathrm{i}}(x_{n+1}) = f^{\mathrm{e}}(t_{n+1}) \tag{3.2}$$

where f^i are internal forces and f^e are external forces.

In order to solve the equation, integration should be considered first. Before continuing into the solution procedure, one should consider the following simplified equation (3.1)

$$M\ddot{u} = f^{e} - f^{i} - f^{d} \tag{3.3}$$

where f^{d} are damping forces.

As mentioned above there are two methods by which an FEA problem can be solved. Through the first numerical scheme, explicit method, the next time step is calculated by using only already known quantities form previous steps. However, during the implicit method, an equation is solved by using the current latter state, which is unknown. Those two methods can be mathematically expressed, considering equation (3.3), as follows,

Explicit
$$U_{t+\Delta t} = f(U_t, \dot{U}_t, \ddot{U}_t, U_{t-\Delta t}, \cdots) \tag{3.4}$$

Implicit
$$U_{t+\Delta t} = f(\dot{U}_{t+\Delta_t}, \ddot{U}_{t+\Delta t}, U_t, \cdots) \tag{3.5}$$

It is obvious that the implicit method is much harder to be implemented as well as it takes more computational effort. That happens, due to the required inversion of the matrix K from equation (3.1). Accordingly, it means that the larger the deformation, the bigger the matrix as well as the computational cost. However implicit have some advantages over the explicit as for its numerical stability and accuracy.

As noted previously, although the **explicit method** is computationally fast it faces some problems with numerical stability, that's why it is said to be *conditionally stable*. That actually means that its solution behavior is not good for too large values of the time step, Δt . Thus, the chosen time step should be for sure less than the critical time step,

$$\Delta t \leq min_e \left(\frac{\Delta x_e}{c_e} \right) = min_e \left(\frac{\Delta x_e}{\sqrt{\frac{E_e}{\rho_e}}} \right) \tag{3.6}$$

where c_e is the material speed of sound and Δx_e is the smallest sized mesh element.

During the **implicit method** though, since unconditional stability exists, it means that in practice a larger step can be used. Of course, that should fluctuate in between reasonable limits and avoid choosing arbitrarily large steps because otherwise high-frequency content in the solution may be lost. Hence, the implicit solver is meant to be used primarily in low-frequency problems in which time dependence is not really important for a solution. Those are static and structural problems. [7]

3.2 Analysis Verification

As mentioned in the previous section, one of the main advantages of implicit method is its unconditional stability. However, not only its computational cost can dramatically increase but also it can encounter some difficulties while trying to reach convergence on a complicated 3D problem, like in sheet metal forming where models are subjected to large non-linear deformations. Hence, in order to overcome those difficulties, the conditionally stable explicit method is used. Although this type of method is usually implemented into short transient and dynamic problems, by applying loads slower, in order to minimize the inertial effects, it can also work for quasi-static analysis. However, by that technique, not only the termination time but also the computational load increases. Hence, in order to minimize that problem, some techniques like time scaling and mass scaling are used, which are actually increasing the loading speed as well as the mass of the elements, respectively. The main target of quasi-static analysis is to apply loads as fast as possible but still having a quasi-static response.

Quasi-Static Approach

It is known that the time increment size is the main reason for affecting the applicability of explicit solutions. Thus, in case one wants to complete an analysis that lasts T seconds, N increments will be performed from the program and each one of them will consist of t seconds duration. The duration of each increment, t, is calculated as follows,

$$t \leq \frac{2}{\omega_{max}} \tag{3.7}$$

where ω_{max} is the highest system eigenvalue.

Hence the total number of increments N is provided by T/t. Due to the fact that a large number of increments actually provoke high computational load, one can try to decrease the CPU time by reducing the total simulation time T or by increasing time increment t. [19]

Time Scaling

The first alternative to reduce the computational load is by decreasing the total analysis time T. This can be achieved by applying loads as well as boundary conditions over a shorter period of time. Such a process may be termed as "**time scaling**" or "load factoring". One way to achieve such a simulation behavior is by increasing the velocity of the forming tool. Nevertheless, that approach can easily give erroneous results if the speed of the process is increased a lot. That happens due to the fact that, as the velocity increases, the kinetic energy of the moving tool is also increasing. Thus, some inertia dynamic effects would be introduced and influence the solution. However, since it is not easy to predict at which level that effect would become significant, there are two ways to make estimations:

The first one, and rule of thumb is to set a limit on the kinetic energy to be less than 5% of the internal strain energy. By this, one can make a rough estimation and observe if the problem has a quasi-static behavior or not.

As for the second way, an also good estimation of the actual amount of load that can be increased is to examine the structural response of the components. This can be achieved by determining the lowest natural mode M of the structure by using an implicit solver. During most quasi-static processes, the deformation of the component occurs over a time period which is much larger than the lower natural mode period. Thus, it is possible for a quasi-static solution to be obtained by increasing the loading rate, provided that time over which load is applied, is much longer than the period of the lowest natural mode. The main advantage of that process is the fact that the mass properties of the structure are not changed so mass-dependent loads and forces don't have to be scaled. [13],[19]

Mass Scaling

The second option could be followed to reduce the computational cost during a quasi-static explicit analysis, is the increase of the stable time step t. This can be normally achieved, by increasing the material density and at the same time artificially reduce the elastic sound speed. Such a procedure is known as "**mass scaling**".

However, the kinetic energy rises while mass scaling increases, like in time-scaling. Thus, there is also a limit to the amount of increased mass, in order to avoid inertial effects. That limit is in fact, that kinetic energy should be less than 5% of the internal strain energy.

One significant advantage of that approach is that the rate at which material is loaded is not affected by changes in the mass density. Hence, rate-dependent material properties can be included. [13],[19]

Apart from the time and mass scaling methods mentioned above, the analysis can also be verified by checking the **force equilibrium** between the applied loads and reaction forces. In case we need to implement a quasi-static analysis, the magnitudes of the applied loads and the reaction forces should be equal. Since the difference between load and reaction are the inertial forces, such an equilibrium can confirm that there no dynamic effects appear inside the simulation.

Energy balance and Energy ratio

Except for the quasi-static verification, an analysis should be also checked from the energy point of view. In general, if the analysis runs properly, the energy curves of the model should be smooth without having any unexpected changes, as well as the energy balance should hold. Thus, concerning system energy conservation, one should investigate the energy ratio of the model.

Before delving deeper into detail, we will take a look at some basics. In general, the total energy in FEA is expressed from the following energy types,

$$E_{total} = E_{kin} + E_{int} + E_{hour} + E_{slid} + E_{damp} + E_{wall} \tag{3.8}$$

where E_{kin} is kinetic energy, E_{int} is internal energy, E_{hour} is hourglass energy, E_{slid} is sliding energy, E_{damp} is damping energy and E_{wall} is rigid-wall energy. Now as for the ratio, it is expressed from the equation below,

$$ratio(t) = \frac{E_{total}(t)}{E_0 + W(t)} \tag{3.9}$$

where E_0 is the initial kinetic energy (all other initial energy is zero) and W external work.

In order to confirm that energy conservation exists, the actual value of the energy ratio should be equal to 1. Now if that value is greater, it means that there is some energy generation inside the system which could impose dynamic effects as well as simulation instability. Nevertheless, we should keep in mind that in complex systems it is common to have a few divergences of the ratio, so it cannot probably reach exactly the value of 1.

3.3 Element Types

Various element families exist, and each one of them is used for a different type of FEA problem, see Figure 3.3. Thus, the two principal element types, as well as the most popular for sheet metal forming analysis, is the solid and shell-type elements. Those choices have been made after discretizing the huge amount of variations in each category.

The first one, standard and simplest to understand, is the **eight-node solid element** sometimes also called "brick element". The incompressibility of that element, something really important for plastic deformation, has provoked its wide use in plenty of structural applications, including bulk-forming. Despite its wide use, there is a major disadvantage during sheet metal forming with that kind of element. This disadvantage occurs due to the fact that usually a number of elements are required through the thickness of the blank, particularly to accommodate spring-back analysis, which results in an enormous number of degrees of freedom and consequently to huge computational time.

Additionally, their spring-back response is not satisfactory due to their high stiffness. Something that improves the whole situation and at the same time provides better bending behavior, is the use of quadratic (high-order) elements with the only consequence that they add further DOF which means more computational load. The difference between a linear, first-order element, compared to a quadratic, second-order element, can be seen in Figure 3.2.

Many variations of a standard brick element have been introduced, with main target to provide coarse meshes without locking (artificial stiffness in certain modes of deformation). On the other hand, these numerical corrections are often introducing the opposite phenomenon, hourglassing, which is a non-physical low stiffness during a certain deformation. Despite those tries of optimization for coarse meshes, the computational load for processes like sheet metal forming stays enormous. [20]

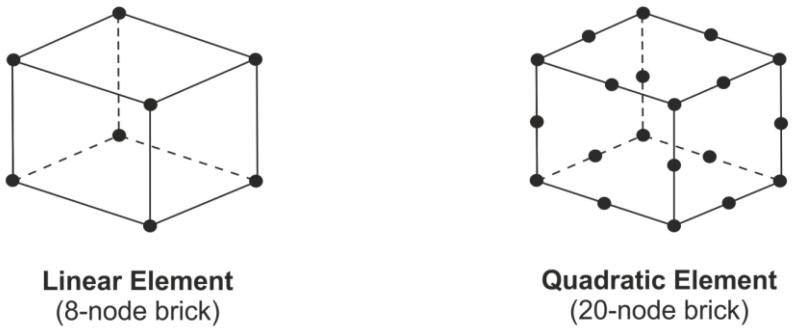

Figure 3.2 Linear vs Quadratic element

By the way, the element type which is mostly used for sheet metal forming analysis is the **thin-shell element** or **simple shell element**. Those elements, are mainly based on a thin-shell theory version, which makes stress and strain assumptions throughout a body. Their shape might be triangular or quad, with the second more frequently used. Those elements don't have any real thickness, so one should keep in mind the important aspect of the clearances between the die faces which could occur a problem. It is common for a shell element that the assumed strain varies through-thickness for evaluating stresses and deformation but usually, the through-thickness stresses are ignored. The shell elements' advantages for metal forming as well as spring-back analysis are much more convincing than those for solids, which are conditionally used for research. Some of the conditions under which solids are frequently utilized are, the critical die clearances, two-

sided contacts, important through-thickness stresses and specific R/t ratios (less than 5 or 6). Apart from those exceptional conditions mentioned above, there is no reason to use solid elements since shells are much more efficient, as well as they provide better results in sheet-forming simulations. [20]

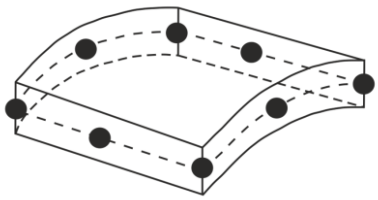

Figure 3.3 Shell element

3.4 Contact Types

During the contact modeling procedure, there are two sides "master" and "slave". The first one is usually considered as a rigid geometrical surface and the second one as flexible, respectively. A contact occurs, through sets, parts, nodes or segments, if there is a possibility of penetration of a slave node to a master segment. By that procedure, after identifying which locations should be checked for this penetration, a contact is being set. [21]

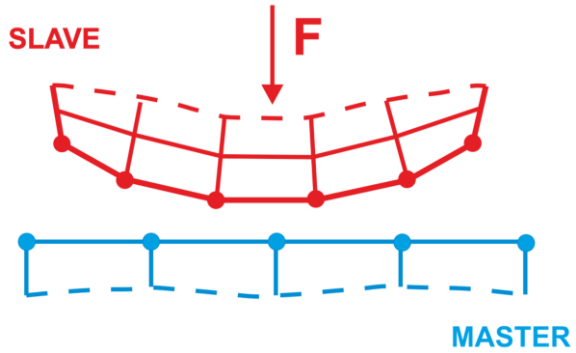

Figure 3.4 The master and the slave side of a configuration. The software is investigating the model to find possible penetrations between the slave side through the master side of the contact.

At every time step, penetration is searched by using plenty of different algorithms. It is common for the contacts search, to be implemented through the *penalty method.* In case a penetration detected, a force proportional to penetration depth is applied and tries to eliminate the penetration. That contact force is expressed by the following equation

$$F_n = k * x_p \tag{3.10}$$

where k is the contact stiffness.

The contact stiffness is calculated in a different way for solids and for shell elements. For shells is given by $k = \frac{sf*K*A}{d}$ and for solids $k = \frac{sf*K*A}{V/A}$, where sf is the scale factor, K is the bulk modulus, A is the segment area, d is the segment diagonal and V the underlying element volume.

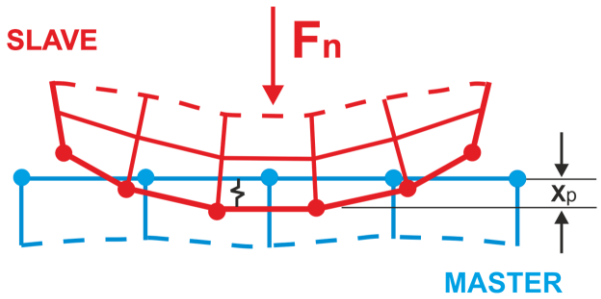

Figure 3.5 The slave side has penetrated inside the master side with a distance of $\boldsymbol{x_p}$, and thus a force will apply in order to eliminate that penetration.

There are two common ways through which one can treat contacts, the first one is NODE_TO_SURFACE and the second is SURFACE_TO_SURFACE.

During the first one, NODE_TO_SURFACE, discrete nodes impact the surface. In this case, master side is defined by segments and slave by nodes. Only the nodes of the slave side are checked for penetration. Looking into a more detailed way, in Figure 3.6, no contact is detected at the same point, since only the slave nodes (blank nodes) are checked for penetration.

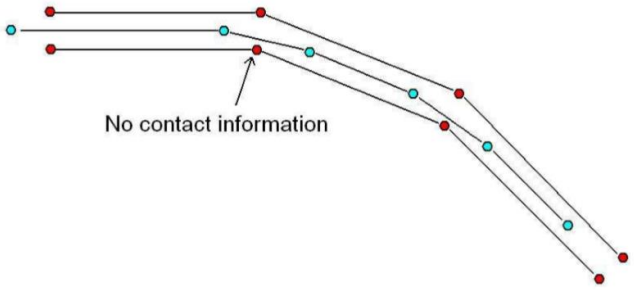

Figure 3.6 NODE_TO_SURFACE contact type [7]

On the other hand, during SURFACE_TO_SURFACE, a surface impacts a surface, see. Now both slave and master sides, are defined by segments and since that contact type is symmetric, both slave and master nodes are checked for penetration. By looking into more detail, in Figure 3.7, a reaction force starts applying only when the tool node penetrates the blank. [7]

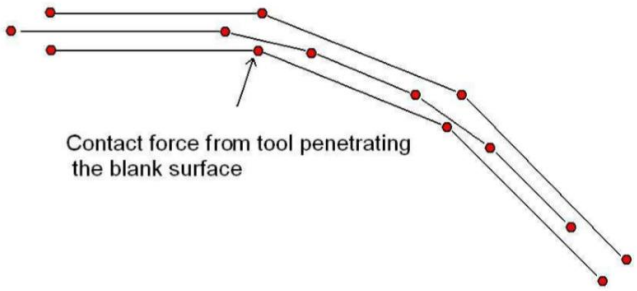

Figure 3.7 SURFACE_TO_SURFACE contact type [7]

3.5 Simulation Methodology

For a simulation setup, one should follow a number of steps through which the preparation, solving, as well as evaluation state will be implemented.

Initially, the design of the model configuration is implemented, and then the rigid tools including the workpiece, are imported into the FEA software pre-processor. The next step is to set-up the mesh and then import material of the FEA model, to define the contacts in between the model parts, the boundary conditions such as loads, velocity,

etc. as well as the elastic unloading phase. After preprocessing finishes, the FEA solver starts to run the simulation. When the analysis reaches termination time, the solution is imported into the post-processor in order to start evaluating the output results which are usually stresses, strains, possible material failures, and springback. In case the results are sufficient, there is no need for modifications so consequently, the validity of the model is confirmed. Therefore, one should proceed to present their values as well as a number of important graphs. On the other hand, if the results are not satisfying, one should return to the FEA model setup, do some modifications to the parameters and rerun simulation. That process should be repeated until decent results are extracted. The whole procedure is summed up and described in the flow chart, Figure 3.8, below:

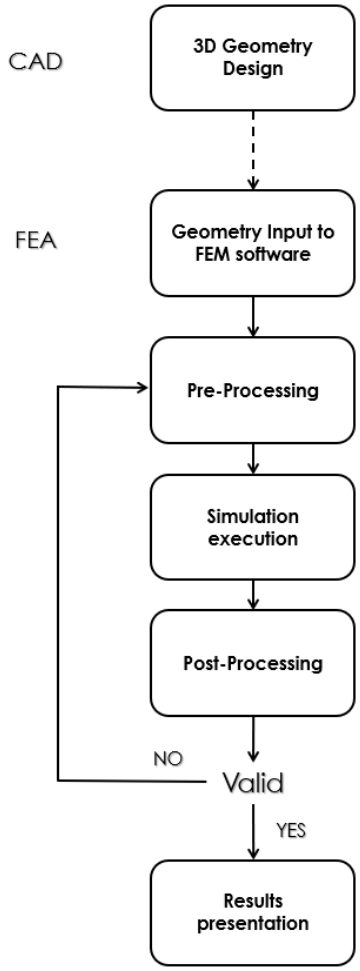

Figure 3.8 FEA model methodology flowchart

3.6 Simulation Setup

Finite element analysis software has been widely used to simulate sheet metal forming processes. Choosing the appropriate FEA module to accommodate a specific forming simulation is something essential. There are plenty of FEA modules that cover a wide range of simulation capabilities. The actual choice depends on the current problem status as well as its complexity. The simulation set up is a really important procedure that could easily affect the accuracy of analysis by differentiating the generated output data results. Thus, one should take care of all the input parameters as well as the solver method that will be used. The steps followed during an SMF simulation are the following:

- CAD geometry input
- Meshing
- Material definition
- Contacts definition
- Boundary Conditions
- Spring-back setup
- Simulation execution
- Analysis verification
- Results evaluation

All those steps can be grouped into 3 sections which are: Pre-processing, Simulation execution, and Post-processing.

Pre-Processing

During a simulation, the pre-processing step is the most important one, due to the fact that before starting with a solving task, it is crucial to be prepared in an appropriate way in order to achieve the desired results. Thus, it is the part where most of the work is being done as well as the decisions made at that stage, will represent and affect the simulation outputs in a high percent.

CAD Geometry input

SRAIL geometry is a quite realistic test that shows all the difficulties typically found in a car part [22], and it is commonly used in automotive industries as a benchmark. After the 3D modeling of S-Rail rigid tools and blank configuration is finished, Figure 3.9 (a), the assembly geometry is positioned in an optimal way, so as to get prepared for the numerical analysis. This can be implemented directly through CAD software or by using the corresponding GUI provided by the FEA. However, the first alternative is much easier to be used. The S-Rail geometry is designed based on mechanical drawings Figure 3.9 (b) from [23] in order one to be capable of making comparisons between those two models.

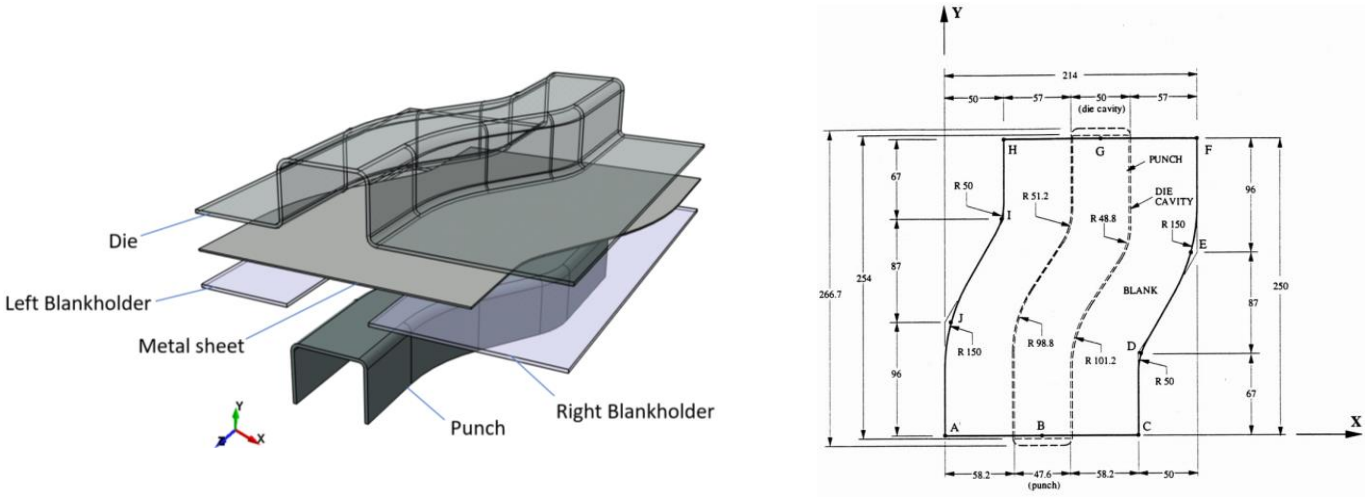

(a) (b)

Figure 3.9 (a) Geometrical assembly configuration of the S-Rail forming process. This is a much more realistic test which shows all the difficulties typically found in car part (b) S-Rail mechanical drawing from **[23]**

As mentioned above, before the geometry is imported into the FEA model, some things should be checked. First of all, the tolerances and clearances between the tools and the blank should be checked and additionally one should confirm that all of the parts are aligned, with respect to the horizontal and perpendicular axis. Consequently, the tools should be positioned in an optimal distance, so as to maintain the sheet metal in between without touching one to another. This happens in order to reduce the displacement of the tool during analysis, as well as to make the solution computationally efficient. After the geometrical check is finished, the whole assembly is converted into a step file, which is a file format designed for geometry exchange between different CAD and FEA software.

Subsequently, the 3D model is imported into the commercial FEA software by using a specific GUI module, which will accommodate the simulation.

Meshing

Generating a good mesh in an FEA model is one of the most important but at the same time difficult tasks during the set-up of simulation, see Figure 3.10. Before proceeding to that step, we have to make sure that everything from the design point of view has been modeled properly in order to eliminate possible geometry issues which can cause difficulties during the simulation.

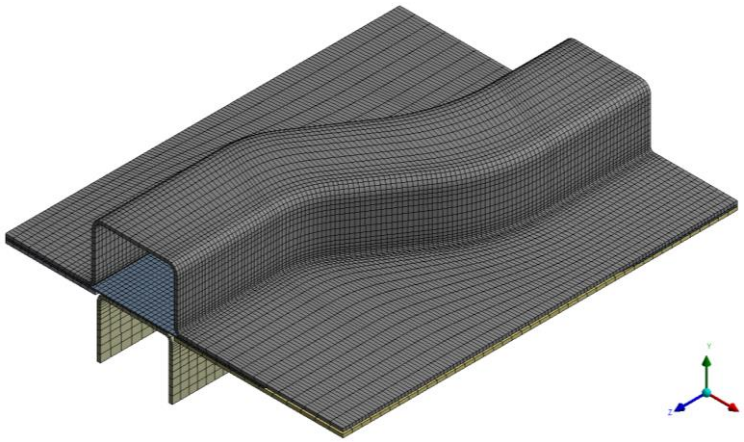

Figure 3.10 S-Rail forming tools and blank meshing into FEA software

In general, a fine mesh is the main target in order to be able to achieve high-quality results. However, that type of mesh consists of a large number of elements, that result in increased computational load. Thus, the optimal solution is to generate a mesh that can provide accurate results but still avoid really small elements that can affect the computational time. A technique that can be utilized in that specific case, is the mesh refinement which will be implemented only in important regions such as in areas with high curvature and leave the insensitive regions with a less detailed mesh. Each one of the assembly parts should be meshed in a specific way as well as with different element sizing depending on the actual accuracy needed from the user. For instance, something that is commonly used in tool meshing, as a rule of thumb, is that every 90 deg curvature of the model should consist of five elements.

Apart from the technique that will be used for the meshing of the model, another important point that should be considered is the element type of the mesh. Regarding the rigid tools, since they are not subjected to large non-linear deformation, the type of element used for the mesh is not so important for results accuracy. On the other hand, the blank should be meshed with caution, due to the fact that it can affect the elicited results of our model. As for the rigid tools, the solid element is used for the meshing of punch, die, and blankholders. Now concerning the meshing of the blank, as mentioned also in section 3.3, it is common for most of the sheet metal forming simulations to use shell quad elements. It has been proved that shell elements are more convincing as well as more efficient for such forming and springback processes, so they can provide better results in sheet forming simulations, [7],[24]. The only disadvantage of that element type is that it doesn't have any real thickness, so the through-thickness stresses are ignored.

In case a better accuracy through blank thickness is needed, some different shell formulations can be used. These are solid-shell elements. By using that specific element type, the accuracy of the model improves since the integration points through the thickness of the simulated blank are increased. Consequently, the degrees of freedom, as well as the computational load, are increasing as well. The corresponding research [23], which is used to compare the results from our analysis, utilizes a solid-shell element type. However, in our case after some trials with solid-shell types of elements, we observed that it is not possible to execute deformation and springback simulations with the optimal mesh refinement because of the limited computational resources as well as due to our analysis, Explicit + Implicit, configuration type (Indication from the FEA software, that the upper RAM usage limit should be increased, in order to be able to implement the springback simulation of our complex problem. That upper limit couldn't be increased, due to software keyword restrictions during that specific type of analysis). A coarser mesh will also affect the plane stress-strain results of both deformation and springback states in our model. Thus, we eventually selected to use the normal shell element for meshing our blank, which of course will decrease the through-thickness accuracy but since the mesh can be finer than the one with solid-shell elements, it will provide better stress and strains results of the surface plane.

Material definition

Proper material selection is really important to acquire accurate simulation results. Inside the FEA model, both rigid and flexible parts will be used. The tools are considered to be rigid bodies on which material doesn't need to be assigned. On the other hand, the material selection of the workpiece is mandatory. During our simulation, since the elicited analysis results will be compared to the already existing values of [23], similar materials should be used. The materials utilized in the research mentioned above, are AL6111-T4 and High Strength Steel (HSS). In order to import the material inside the FEA analysis, we will first model the elastic region by using the following parameters: Density ρ, Young modulus E, and Poisson ratio v, while for the plastic region, a nonlinear isotropic hardening function will be utilized. The hardening function is the following,

$$\sigma_y(\kappa) = \sigma_{yo} + Q(1 - exp(-\beta\kappa)) \tag{3.11}$$

where σ_{y_0} is the initial yield stress, Q is the maximum change in the size of the elastic range and β is the rate of change of elastic range size. The values of those parameters are provided in Table 1.

Material	$\boldsymbol{\rho}$ (g/cm^2)	**E** (N/mm^2)	**v**	$\boldsymbol{\sigma_{y_0}}$ (N/mm^2)	**Q** (N/mm^2)	β
AL6111-T4	2.71	69000	0.33	161	207	9.74
HSS	7.85	206000	0.3	355	260	9.79

Table 1 AL6111-T4 and HSS material elastoplastic properties

The material model will be used for that analysis, is *MAT_PIECEWISE_LINEAR_PLASTICITY (*MAT_024). Considering those material properties already provided and the stress-strain curve displayed below, see Figure 3.11, the Ultimate Tensile Strength actually reaches 368 MPa for AL6111-T4 and 615 MPa for HSS.

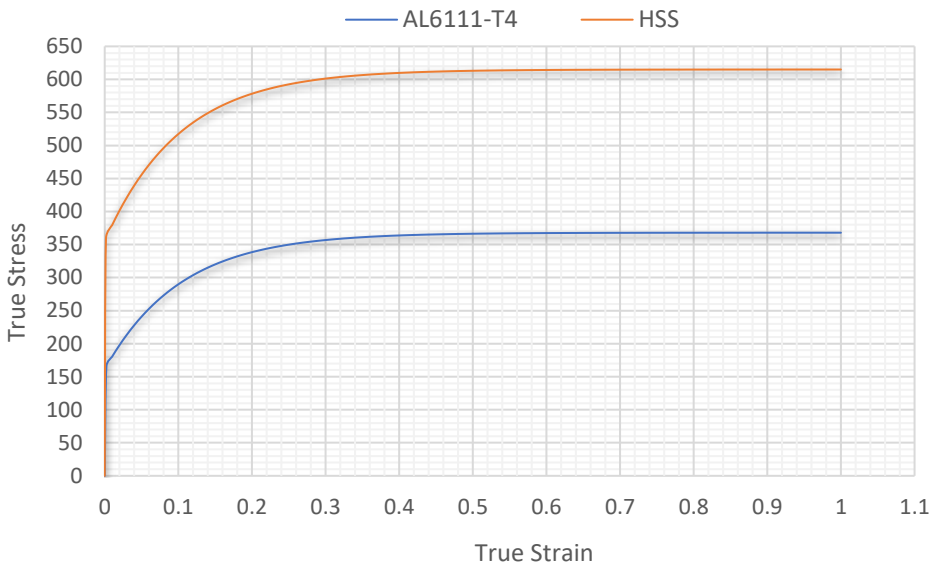

Figure 3.11 Stress-Strain curve for AL6111-T4 and HSS material

Contacts definition

One very important section of the analysis is contact modeling. In case a simulation fails, plenty of the times the error can often be related to problematic contacts. There are many types of contacts in FEA software but only some of them are commonly used in sheet metal forming analysis.

First of all, the type of contact used between the forming tools and the blank is frictional, while the friction coefficient for AL6111-T4 is $\mu_c = 0.10$ and for the HSS is $\mu_c = 0.11$. Concerning the contact properties, as mentioned also in section 3.4, there are two ways mostly used to treat contacts. However, when the mesh from the master side (forming tools) is finer than the one from the slave side (blank), there are possibilities of blank penetrations inside the rigid tools. In case of such a condition, it would be much better to use SURFACE_TO_SURFACE contact even though is more computationally costly. In our case, the rigid tools mesh is refined in each tool curvature with 4-5 elements over the radius, so it gets finer than the mesh of the blank in those specific areas. Thus, we will use the SURFACE_TO_SURFACE contact type in order to avoid penetration issues. [25]

Boundary conditions

When the meshing of the geometry is completed, the next step is related to the boundary conditions setup. After positioning all the assembly parts in an optimal way and arrange all the pre-processing stages mentioned above, one should take care of the rigid tool constraints, the applied loads, as well as their motions which are used to perform the sheet metal forming processes. Despite the fact that the procedure is quite straightforward, some details should be considered beforehand.

First of all, we will take a look at the tool motions. Generally, it is better for a tool movement to be expressed by forces, but due to the fact that they are usually unknown, users are compelled to use prescribed tool motions. Hence, in our simulation, the "punch" movement will be expressed by velocity.

The actual amount of velocity increase varies in each simulation and it basically depends quite a lot on the 3D model's details, such as the material, blank thickness, geometry size, etc. A general recommendation that will provide better results and eliminate dynamic effects, is to use a trapezoidal velocity, see Figure 3.12. By using that velocity profile, during the start of the procedure, the tool will hit the blank in a smoother way, as well as the tool speed will be reduced at the end of the simulation. [26]

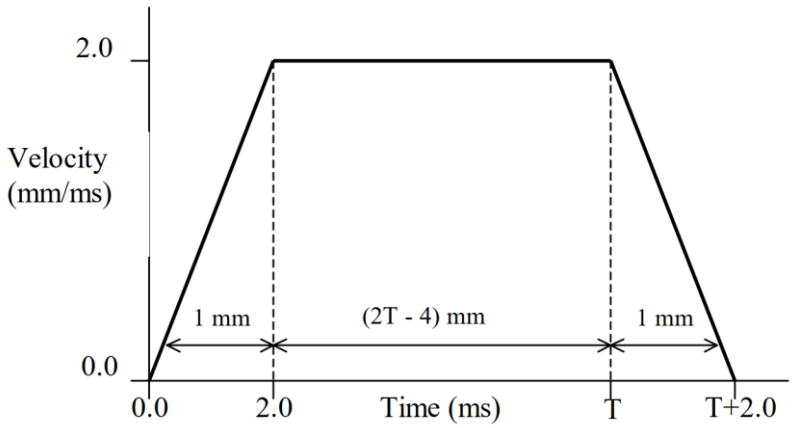

Figure 3.12 A trapezoidal punch velocity profile **[26]**

During a simulation, the computational load depends on the actual speed of the tool which is usual in reality to be rather slow. Slow tool velocity corresponds to large end time and as a consequence to increased computational load. Thus, as also mentioned in

section 3.1, time-scaling is something that is usually implemented in such processes and aims to numerical load reduction. However, such an increase in simulation velocity can possibly introduce dynamic effects which can result in the continuous moving of the blank due to inertia and as a consequence to output data distortion. Hence, the specific technique should be used with caution and only if these problems referred above are neglected. Now, in our case, targeting to reduce the numerical load, time-scaling will be used and thus the "punch" velocity of the analysis will be increased. Thus, the tool speed will rise from 5 mm/s (punch velocity used in [23]) to 468 mm/s, see Figure 3.13. That velocity increase has been established after making the appropriate verifications to confirm that no dynamic effects appear.

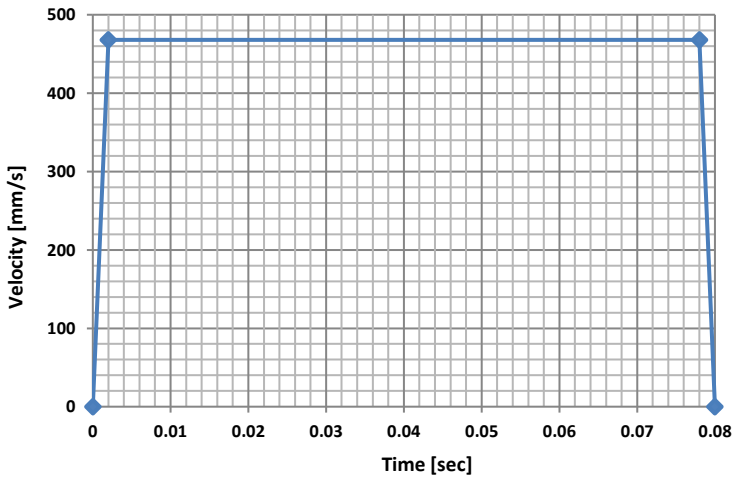

Figure 3.13 Trapezoidal punch velocity profile used during analysis with max velocity V=468 mm/s

Apart from the velocity setup, something also important to be considered, are blank-holder forces (BHF), see Figure 3.14. That part of the model is used in order to stabilize the workpiece during the forming procedure. One should be cautious while applying BHF, because either being larger or smaller than needed, they can cause some problems by generating material failures to the specimen and reduce the quality of the results. In our case since we will make a comparison with some already existing results from research [23], the BHF values will be preserved the same, as in the corresponding simulations with which a comparison will be made.

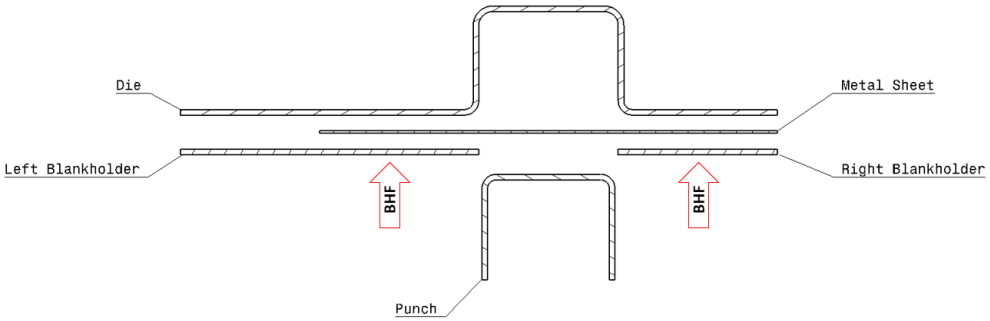

Figure 3.14 Blankholder forces applied to the specimen (S-Rail assembly cut section)

Springback setup

There are various ways of simulating springback using both explicit and implicit algorithms but it is common for the standard explicit dynamic method to be avoided in that specific process because it can easily cause dynamic oscillations. Since our main target is to obtain a static spring-back solution without any dynamic effects, the static implicit method will be chosen instead of the explicit one. However, by getting into more detail, there are more than one different implicit spring-back methods but at this specific study, the seamless method will be used.

During that method, the forming analysis procedure begins with an explicit method until full deformation is reached. When the dynamic part finishes, there is a switching point where the analysis changes seamlessly, in an automatic way, to implicit spring-back simulation. During the spring-back setup, the user should define the retained bodies and all of the other remaining bodies will be deleted after the simulation reaches the switching point. Usually, during that type of simulations, the retained part is the sheet metal blank, based on which the spring-back will be studied. On the other hand, the bodies which will be deleted, are rigid tools such as punch, die, and blank holders. Then, apart from the already mentioned, the contact interfaces which were used during the explicit blank forming state, are also deleted from the model. [27]

Now in order to be able to run that implicit springback simulation, one should set up the process by using software integrated keywords that are actually applied to the solver through a specific feature called keyword snippet. Those keywords provide access to a

flexible and logically organized database, containing a number of functions working on the backstage of the FEA software so as to prepare and activate the simulation.

To start with, as mentioned above the implicit springback phase begins after the forming simulation reaches the end time. Thus, in order to specify the actual point in time, until when the forming simulation runs as well as Implicit analysis starts, we utilize the keyword *CONTROL_TERMINATION. The default choice is 2.0*ENDTIM. [28]

After the termination time is defined, the next step is to determine the constraints during the springback phase. While the static springback phase is simulated, the part must be constrained by defining a number of essential boundary conditions in order to avoid rigid body motion. The main reason for constraining the metal blank is to avoid inertial effects in the static analysis which could result in blank moving as a unit in space without deforming. Hence, the part should be constrained in six directions which means in the three translations and three rotations. These constraints define a reference point of the blank which remains fixed when spring-back deformation occurs as well as ensures that the stiffness matrix is non-singular. Since all the displacements of the workpiece are measured relative to that specific constrained point, it is necessary to be chosen correctly in order not to affect the sprung piece shape. A typical method to select the appropriate constraints is described in Figure 3.15 and recommends to select three points which are well separated from each other and far from edges.

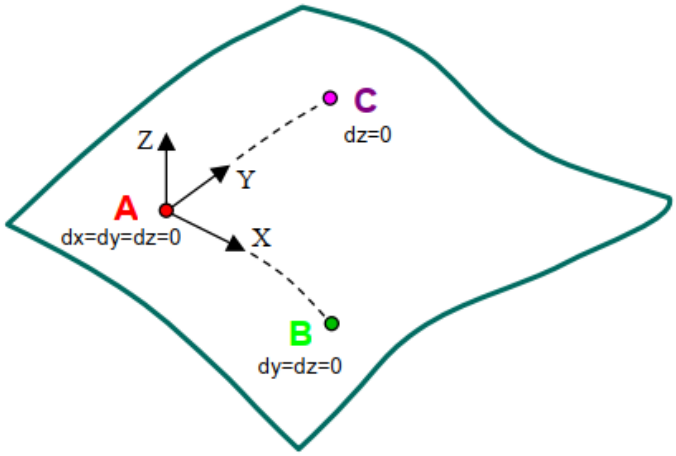

Figure 3.15 Diagram showing the constraint nodes location for a typical springback model. Through node A, all of the translational body motions are constrained and then by containing nodes B and C the rigid body rotations are eliminated as well. [27]

It is obvious that many possible boundary condition combinations can be used so as to eliminate the rigid body motion. Through that example, one simple method to define the minimum possible constraints is presented. However, one should pay attention to the number of constraints because in case more than appropriate are implemented, springback deformation can be suppressed or altered [29]. Hence, these boundary conditions of the spring-back phase can be added via the *INTERFACE_SPRINGBACK_SEAMLESS keyword. [29]

By aiming to make the springback results more accurate, a non-linear solver must be used. Usually, the elastic unloading simulation converges without difficulty. However, in some specific simulations springback is particularly difficult to be computed due to non-linear deformation, dynamic material response or numerical simulation errors. Hence multi-step spring-back simulation is automatically invoked which means that the spring-back deformation is divided into smaller, easier to manage, steps. The keyword *CONTROL_IMPLICIT_GENERAL is used to activate implicit method as well as to choose the desirable time step size. Afterward, in order to be able to select between linear or non-linear analysis types and in parallel define the convergence tolerances, *CONTROL_IMPLICIT_SOLUTION keyword should be used.

The applied load in a springback simulation results from the initial stress in the metal specimen, which due to rigid tools removal is no longer in equilibrium. For challenging spring-back problems, the load must be applied slowly over several steps, in order to make the non-linear spring-back more manageable. This could be achieved by artificial stabilization, which is a method that distributes spring-back response into several steps. During that method, the motion of the sheet nodes is restricted by using artificial springs. As solution proceeds, the stiffnesses of the springs are reduced and step by step more spring-back is allowed to the model. Once the termination time is reached, springs are completely removed and unrestrained spring-back is allowed. That happens only when the solution is about to finish, otherwise some artificial stabilization will remain inside the model and results will not be accurate. That procedure is be activated through the use of *CONTROL_IMPLICIT_STABILIZATION keyword. [27]

Finally, in case convergence problems occur, for guiding the solution to the termination time as quickly as possible, the automatic time step control is used. This is activated through *CONTROL_IMPLICIT_AUTO keyword by which it actually retries steps

persistently in places where the equilibrium search has failed until the termination time is reached. [26]

Simulation Execution

Once everything is ready and all boundary conditions are set up properly, it is time to execute the analysis. As mentioned above, the analysis consists of two phases, the explicit deformation, and the static implicit springback. When the first phase reaches the termination time, the software switches automatically to the second process which is elastic unloading.

Post-Processing

After the simulation solution process finishes, post-processing and results evaluation are the following steps. In general, as in every simulation process, also in sheet metal forming analysis, there is a high interest in evaluating the whole procedure by checking some important results. Although after a simulation solution there is a large number of outcomes that can be evaluated, in reality only a few of them can raise the interest, such as stresses, strains, thickness reduction and forming limit diagram. Additionally, during metal forming simulations, it is essential to evaluate the springback effect as well, which is a really important part of the analysis. Nevertheless, before reaching that state, it is mandatory to make some verifications concerning the behavior of the model.

Analysis verification

First of all, in order to confirm that no artificial effects are introduced into the simulation, the quasi-static behavior of the model is verified. During that process, the kinetic/internal energy ratio, as well as the equilibrium between the loads and reaction forces of the tools and blank, are investigated. In case the ratio value is less than 0.05 and an equilibrium between the loads and reaction forces of the model exists, respectively, there is first good feedback concerning the model behavior.

Subsequently, we proceed in the quality estimation of the analysis by checking the punch force/stroke curve of our model. As such, we can observe whether the force applied from

the punch to the specimen during the tool traverse is reasonable, through which we can confirm if the pre-processing state of the model is defined properly. In the case of unrealistically large forces or extreme behaviors, some issues may occur. Usually, that kind of problem appears, due to the fact that tools are set to traverse more than the normal distance and a through-thickness compression on the blank is achieved. However, sometimes those large reaction forces could also imply a problematic geometry.

Last but not least, an evaluation of the model energies is implemented. During the final step, in order to check that the simulation runs sufficiently, we evaluate the energy conservation of the model. This can be accomplished by checking if the model's energy ratio is equal to 1 or really close that value especially when complicated models are simulated. If so, it means that our model satisfies energy conservation and no additional energy is generated. In case the energy conservation does not hold, then one should check if any contact issues exist. Additionally, by looking into the energy summary plot, the internal energy of the model should be for sure much bigger than the kinetic and all of the energy curves should be smooth without any steep parts and jumps.

Results evaluation

After the analysis verification of our model, we continue with the investigation of the stresses, strains in order to confirm that the values presented are reasonable. Then we proceed in evaluating the actual state of the blank and detect any possible failures after the deformation such as cracks, risk of cracks or wrinkles. The most common way to detect such material weaknesses is to evaluate the thickness reduction plot. By taking a look into the thickness reduction percentage of the formed blank, one can take a first impression concerning the most vulnerable areas of the specimen. However, in order to acquire more detailed and accurate results, the Forming Limit Diagram and the strain distribution plot should be considered. Subsequently, after the forming process evaluation finishes, the next important step is the springback effect assessment. To quantify springback, we consider some section cuts on the specimen, along which the elastic unloading prediction is implemented.

Thus, if the analysis meets all of those conditions mentioned above, one could say that it runs properly and the elicited results should be pretty much accurate.

Chapter 4

Results

In this chapter, the elicited results from the simulations modeled in the previous section will be presented, while considering the S-Rail analysis results from [23] and make a comparison between them. Those models will be compared, in order to define the actual error percentage between them. The first simulation run will be implemented by using as a material, Aluminum 6111-T4 and after that, we will run a second analysis by using an HSS. Afterward, we will make some modifications to our simulation model parameters in order to implement a springback sensitivity evaluation. In order to carry out the simulation, a commercial FEM simulation software will be used and in combination with some python customization tools, a connection with LS Pre-post will be established for visualization purposes.

4.1 AL6111-T4 material

During that section, we will implement FE analysis by using AL6111-T4 and BHF equal to 10KN. Then the elicited forming and springback results will be compared with the corresponding outputs from research [23].

Analysis verification

Initially, the actual behavior of our model will be investigated, in order to confirm that our elicited results are not distorted from dynamic effects.

Quasi-static behavior

After the analysis termination time is reached, one should verify if the analysis has a quasi-static behavior. The two main verification approaches are: Kinetic/internal energy ratio and Force equilibrium.

As for the **Kinetic/internal energy ratio**, it's a first rough estimation of the simulation. In case the ratio is less than 0.05, one can define that dynamic effects don't impact the simulation results. In our case, as can be seen in Figure 4.1, the kinetic/internal ratio is nearly zero except for the steep increase between 0 and 0.0044 sec which reaches a maximum of 1.652. Of course, the ratio equal to 0.05 cannot be true for the whole analysis but should hold for most of the time, which is the fact is followed in our analysis plot. As such, it seems that we receive good first feedback concerning the quasi-static behavior but it is not of course enough since some other parameters should be also investigated.

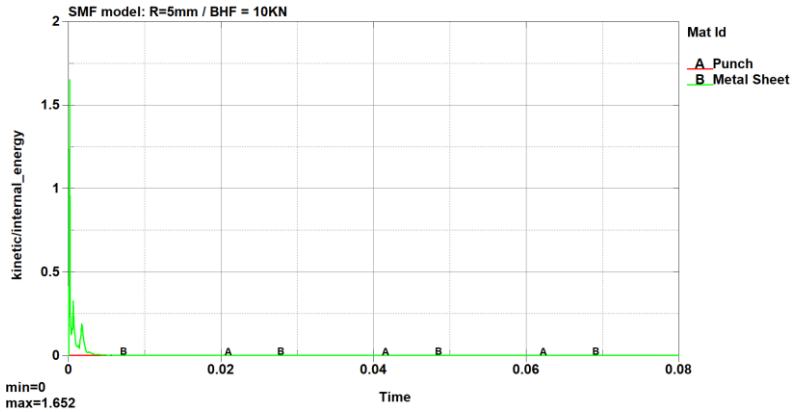

Figure 4.1 Kinetic/Internal energy plot

Now regarding the second verification approach, we have to check the **Force equilibrium** between the punch and the metal specimen, in order to acquire a better understanding of the overall model behavior. As already known, in a static analysis there are no inertial

effects, so an equilibrium between the applied load and the reaction forces exist. Now as mentioned already, in quasi-static analysis, since the actual difference between a load and a reaction is the inertia forces, an equilibrium between those two should exist and confirm that the simulation has the desirable behavior. Even though that method is adequate to show if our analysis has the needed behavior, sometimes there can still be local effects that don't show up in global force balance. Hence, one should increase the simulation termination time and after that, check the new extracted results to see if any changes appear.

In the beginning, the forces with initial termination time equal to t=0.08 sec will be studied and afterward, we will double the end time t=0.16 sec in order to confirm that the simulation maintains the desirable behavior. We should keep in mind that by increasing the termination time and keeping the same tool traveling distance, the velocity will be decreased. Hence, at the first simulation, the tool moves with a velocity of V = 468mm/s but in the second one, the velocity decreases to V = 231mm/s.

By investigating the punch and reaction forces of our first simulation with ending time equal to t=0.08 sec, see Figure 4.2, we can observe that the difference between them is really small, nearly negligible. As such, we can understand that almost all the energy produced from the punch is received from the blank without important losses. Hence, by considering those results one can say that no inertial effects should be present inside our model.

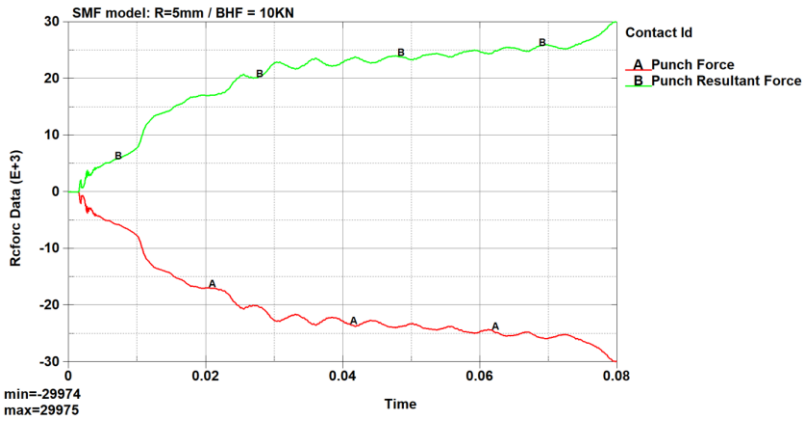

Figure 4.2 Punch and resultant force of model with initial termination time t=0.08sec

However, as mentioned previously, due to the fact that some inertial effects may not appear during that force balance, we will evaluate a second run of the exact same model with the only difference of doubling the end time (t=0.16 sec). So, by taking a look at our new load/reaction forces plot, see Figure 4.3, we can observe again a similarity between them. Therefore, after a second confirmation, one can definitely claim that the model has a quasi-static behavior, so no dynamic effects should show up.

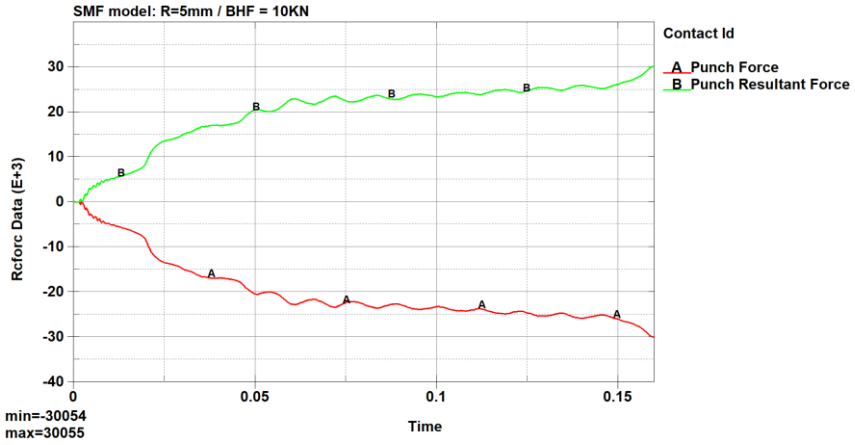

Figure 4.3 Punch and resultant force of model with termination time t=0.16sec

Punch Force/Stroke assessment

In order to make a quality estimation of the analysis, a comparison of the punch forces and punch displacements of our model can be made, based on the corresponding results of [23]. As we can observe, the experimental values of the punch force vs displacement diagram in Figure 4.4, are within a minimum of 21 KN and a maximum of 27 KN (EB 2.07 is dismissed). The research simulation achieves a force curve laying in between those two borders with a maximum of ~ 23-24 KN. Now by taking a look in our punch force vs displacement curve, it reaches a maximum of 29.6 KN. In parallel, by observing the overall path of our analysis curve one can define that it is offset with an average of 3.8 KN nearly all of the punch motion, compared with the simulation curve of [23]. Last but not least, the actual percentage error between the max value of our plot curve and the upper border of the experimental values is nearly 9.6 %.

Something also important to be pointed out, is the instability of our initial curve in comparison with the one from [23], possibly due to some higher frequency oscillations,

which are generated due to the dynamic analysis method. Since those are not useful for the evaluation of the results, we can filter them and make the curve smoother. This could be done, by using a Butterworth filter of 100Hz through which we allow only lower frequencies to come through.

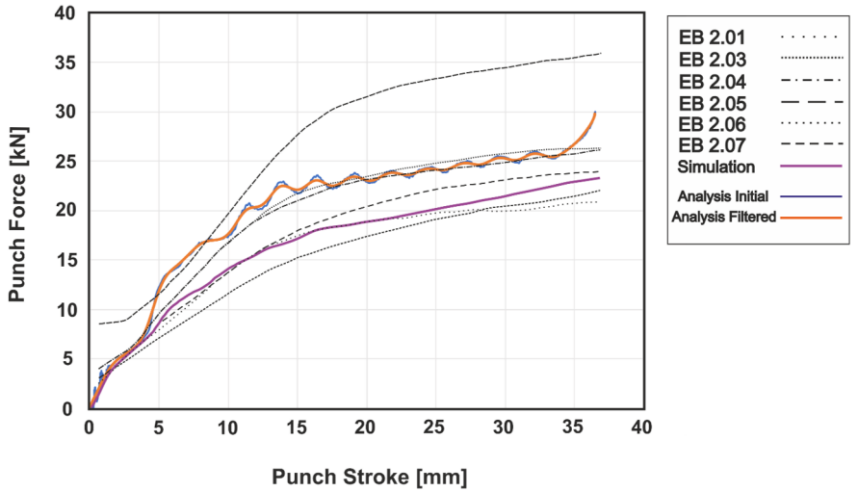

Figure 4.4 AL6111-T4, BHF=10KN, Punch Force vs Punch stroke comparison between analysis and [23] results.

Energy ratio and Energy balance

Now by looking into the ratio plot of our simulation Figure 4.5, one can easily define that the energy ratio is 1 or really close to that value which means that our model satisfies energy conservation and doesn't generate any additional energy. Thus simulation runs properly.

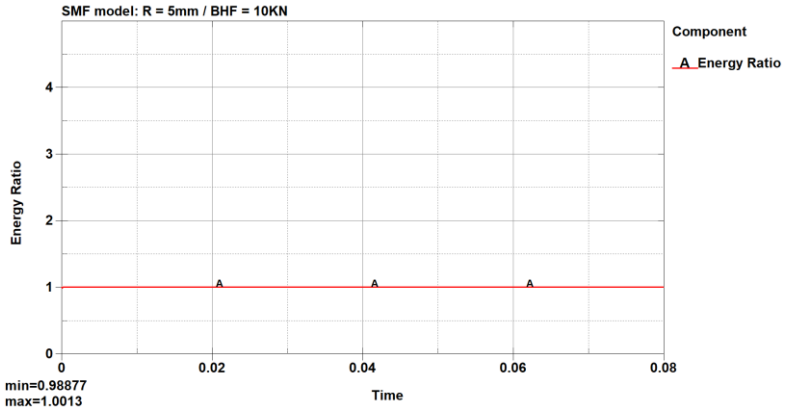

Figure 4.5 Energy ratio plot

In addition, we investigate the general energy plot, see Figure 4.6, which contains all of the existing energies of our model. Since those curves are smooth without any jumps, as well as the kinetic energy of the model is much less than the internal energy it is confirmed once more, that the energy conservation is adequate. [30]

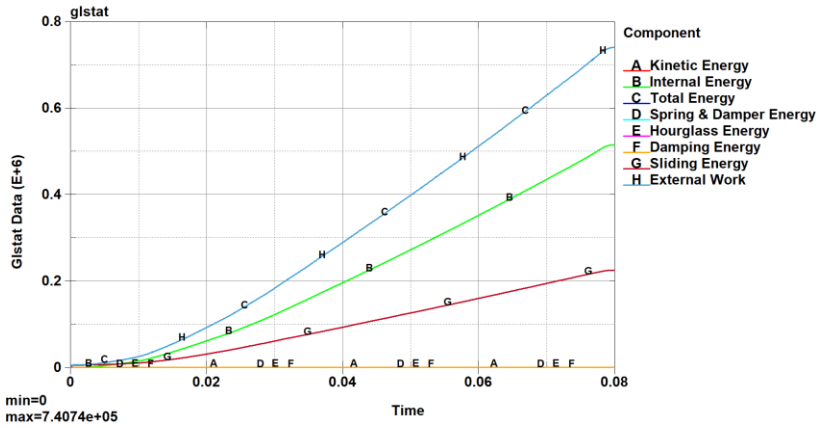

Figure 4.6 Energy summary plot

Forming process results

After receiving satisfying results related to both quasi-static behavior and energy conservation of our analysis, we will proceed to our actual post-processing results presentation. Our S-Rail model results will be compared with the existing plots and values from the already published research [23] in which a common S-Rail study was conducted. In that way, we can check if our analysis outcomes are meaningful. Thus, we will investigate the effective stresses, the plastic strains and then we will compare them with the values of research. Afterward, the thickness reduction of the metal sheet, as well as the FLD and the strain distribution diagram will be evaluated, in order to show the failure and thinning state of the model.

Before continuing with the comparison between our simulation and the results from [23] we should go through a procedure of defining the similarities as well as the differences between those two models:

First of all, as for the differences, one of the most important is the **FEA techniques** used to solve the simulation. In research [23], both deformation and spring-back processes are

simulated through the implicit method, whereas in our case, explicit analysis is used for the deformation process and implicit analysis for the springback operation.

Additionally, there is also a difference concerning the **velocity of the forming tool**. The constant traveling speed of the punch used in [23] is 5 mm/s while in our model is 468 mm/s. In fact, the higher velocity in our simulation targets to minimize the computational load. The elicited results were checked through verification techniques in the previous section, and as such, it was proved that no dynamic effects appear in our simulation after that analysis speed increases.

Last but not least, one more detail which is different between those two simulations is the **element type** used for the blank meshing. As mentioned in section 3.6, due to limited computational resources as well as due to our analysis configuration type (Explicit + Implicit), we used the normal shell-type element instead of a solid-shell type. This will decrease the through-thickness accuracy of our model but at least we could have better plane stress-strain results since we can achieve finer mesh by using the normal shell element.

Apart from those differences stated above, everything else used in our simulation is the same as in research [23].

Effective (Von-Mises) Stress

To begin with, the first step of the results' evaluation contains the effective stresses of our model before springback. By looking into Figure 4.7, the maximum effective stress of our model is 317.5 MPa. This is lower than the material UTS, which is 368 MPa so we are in a safe area without having possibilities of necking or even crack failures. In the meantime, the max effective stress values of [23] reach 275 MPa, which results in a percentage error of 15.4% between them.

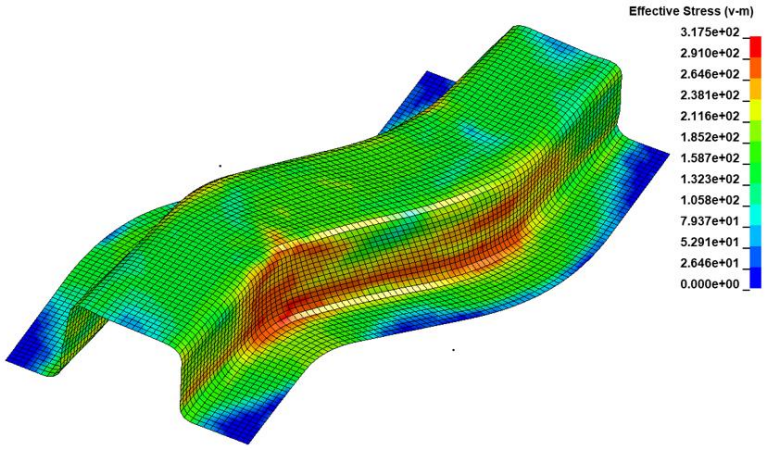

Figure 4.7 AL6111-T4, BHF=10KN, Effective von-Misses stresses plot before elastic unloading

Subsequently, the effective stress distribution after elastic unloading will be studied. As can be seen from Figure 4.8(b), the max effective von-misses stress of our model reaches 238.8 MPa, whereas in [23], roughly estimating from the visualization plot, the max stress is around 206.3 MPa. By evaluating and comparing those max stress values, the approximate percentage error between them during that state reaches around 15.4%.

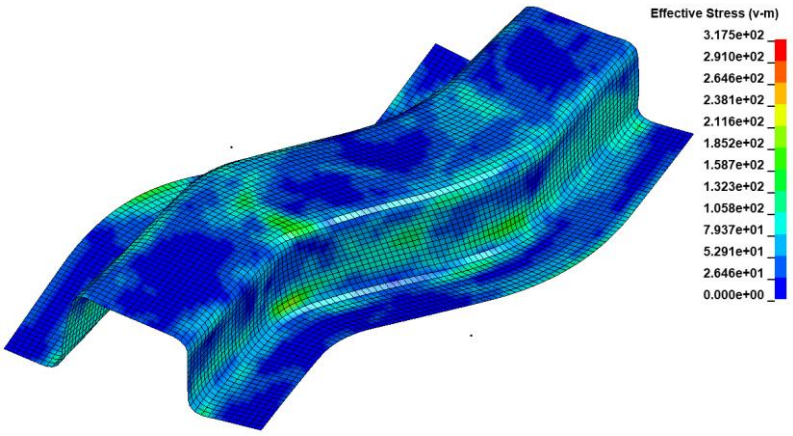

Figure 4.8 AL6111-T4, BHF=10KN, Effective von-Misses stresses plot after elastic unloading

Effective Plastic Strain

After evaluating and comparing the effective stresses of the model, we should also investigate the plastic strain of the workpiece since is also a very important part. We can observe that in our model, see Figure 4.9, we reach a maximum plastic strain of 0.2275

instead of 0.207 that model from [23] displays. By evaluating and comparing those max plastic strain values, the approximate percentage error between them is 9.9%.

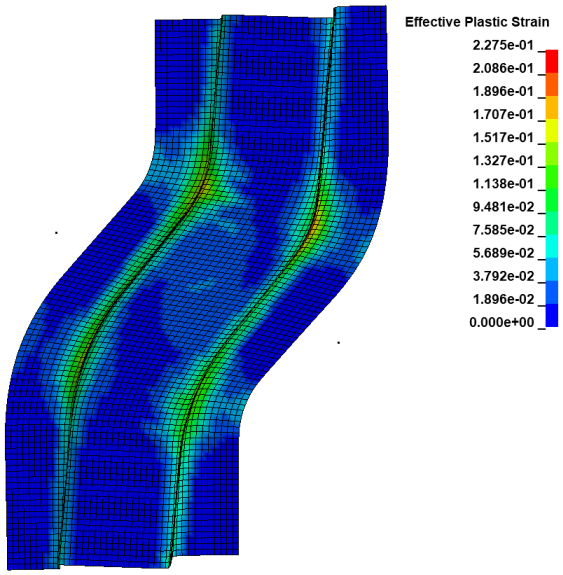

Figure 4.9 AL6111-T4, BHF=10KN, Effective plastic strain plot

Material Failures evaluation

To evaluate the simulation concerning the workpiece failures, one should refer to the **thickness reduction plot** as well as the **FLD** and **strain distribution diagram**. Through both of them, a good estimation can be made regarding the load that the specimen can withstand until some cracks appear.

In fact, by taking a look at the thickness reduction plot below in Figure 4.10, we can observe that the thickness is within a range of -7.65 to 7.75 % of the initial specimen thickness, which is 0.92mm. From a first look, it seems that the material thinning is not that high to provoke cracks on the metal workpiece. In order to confirm that this prediction is right, we have to also study the FLD plot as well as the strain distribution diagram.

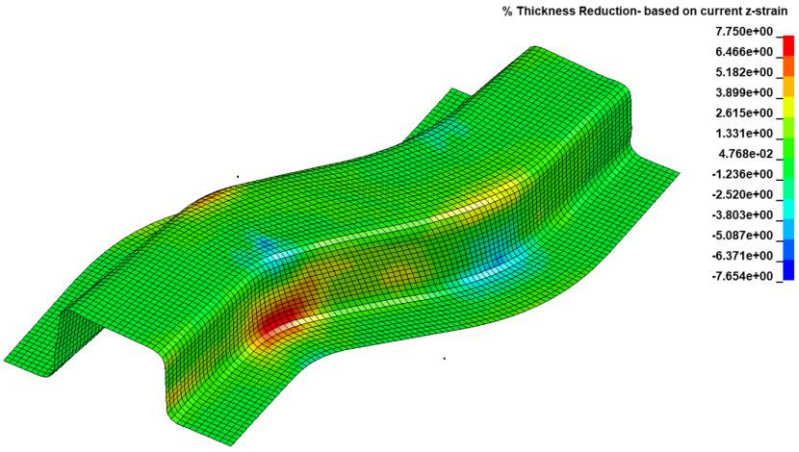

Figure 4.10 AL6111-T4, BHF=10KN, Thickness reduction plot

By taking a look at the FLD plot and the strain distribution diagram, Figure 4.11(a)(b), we can get an idea about the amount of thickness reduction the material can withstand before any cracks occur. From the first look on those plots, we can see that there is no indication for cracks, not even for risks of cracks which is a very good sign. Such results seem to be reasonable and by combining them with the low material thinning values, the assumption made at the beginning is confirmed. Now apart from the specimen thinning, something also important to notice is the negative thickness decrease or thickening. By looking in our model, there are many wrinkled areas as well as many areas that tend to wrinkle. If one checks again the thickness reduction plot Figure 4.10, it can be observed that indeed most of the wrinkling failures occur where thickening is indicated. However, to further investigate those results, we can detect exactly where those wrinkles exist on the model, by observing the plain geometry in Figure 4.12. Hence, one can see that some of the wrinkling areas indicated by the FLD, doesn't even exist on the model surface. So, one can conclude in the fact that forming limit diagram should be used with caution when it comes to wrinkling evaluation because sometimes it can miss some of those indications.

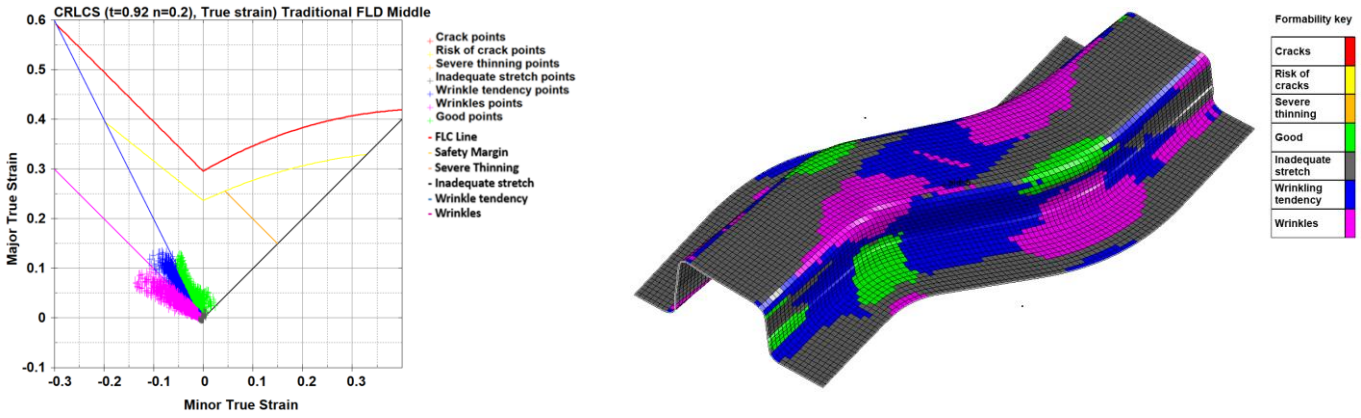

(a) (b)

Figure 4.11 AL6111-T4, BHF=10KN, (a) Strain distribution plot in forming simulation, (b) Forming Limit Diagram (FLD) plot

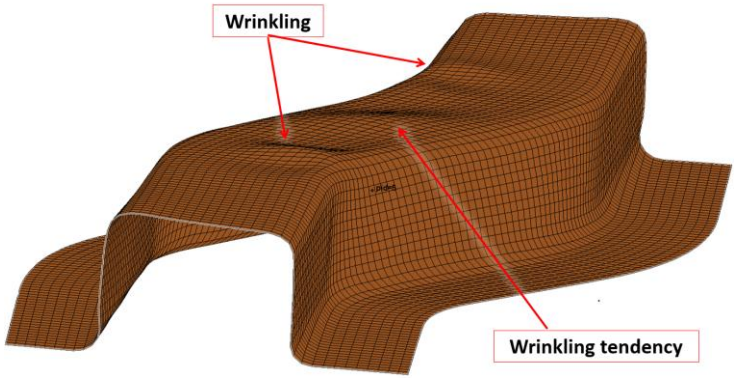

Figure 4.12 AL6111-T4, BHF=10KN, Plain geometry with wrinkling indications

Springback prediction

After the forming process finishes, the next step is springback evaluation. The material, as well as the BHF of the model, remains the same. To quantify springback, two path lines J-D and I-E were considered, see in Figure 4.13 (a). One section cut will be applied per corresponding path line. Afterward, along these section cuts, "before springback" and "after springback" states will be plotted. Additionally, a comparison between the "after springback" states of specimens will be made, based on the results of our analysis and those from research [23], see Figure 4.13 (b).

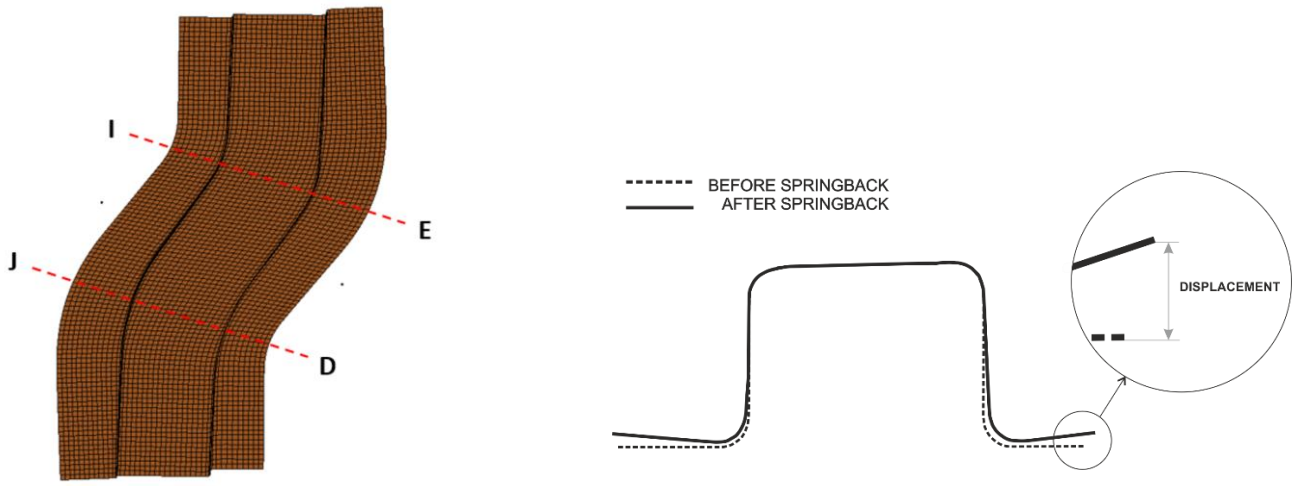

(a) (b)

Figure 4.13 (a) J-D and I-E section cut paths (b) Blank displacement measurement, between "before and "after" springback states. Implemented on both sides of each specimen's section cut.

To start with, we will study the first section cut, along the path J-D. The material used remains AL6111-T4 and the blankholder force as well, equal to 10KN. By looking into Figure 4.14 (a), we can observe that the geometry of the blank changes after elastic unloading in our analysis. Subsequently, in Figure 4.14 (b), a comparison between the "after springback" states of both our analysis results and the ones from [23] simulation, is implemented. As we can see, the displacement differences are 0.16mm and 0.26mm, for the J and D section side, respectively.

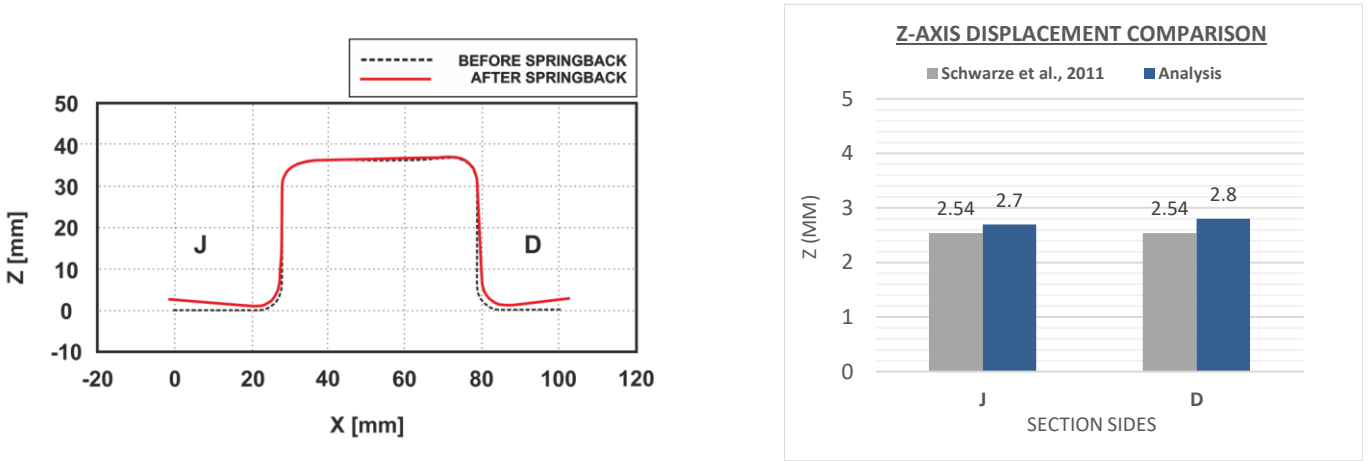

(a) (b)

Figure 4.14 AL, BHF=10KN, (a) Workpiece deformation before and after springback in section J-D (b) After springback z-axis displacement comparison between **[23]** and Analysis.

Afterward, we will investigate the second section cut, along the path I-E. By looking into Figure 4.15 (a), we can observe again the displacement in our model between, "before" and "after" springback states. Subsequently, in Figure 4.15 (b), we make again a comparison between the "after elastic unloading" states of our analysis and the corresponding simulation from [23]. As we can see, the displacement discrepancies are 1.17mm and 2.02mm, for the I and E section side respectively. One can observe that the displacements along the I-E path, are larger than those along J-D.

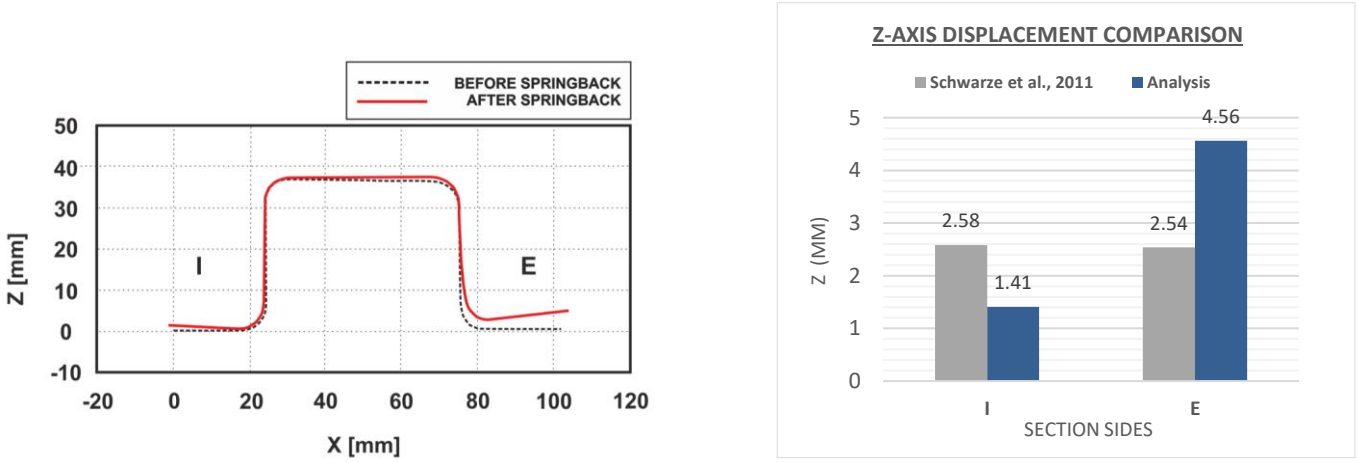

(a) (b)

Figure 4.15 AL, BHF=10KN, (a) Workpiece deformation before and after springback in section I-E (b) After springback z-axis displacement comparison between **[23]** and Analysis.

4.2 HSS material

In that section, the analysis will be conducted by using a different material, HSS as well as a larger BHF equal to 200KN. Considering those modifications, as for the dynamic deformation simulation phase we will investigate the possible differences between the current and the previous analysis data, using AL6111-T4, because no plots are presented for that specific state in [23]. However, as for the springback prediction, we will compare the elastic unloading values of our analysis, with the corresponding ones from research [23].

Analysis verification

Initially, the actual behavior of our model will be checked, in order to confirm that our elicited results are not affected by inertia.

Quasi-static behavior

As mentioned in the previous section, our explicit analysis should have a quasi-static behavior which means that no dynamic effects should exist inside our model. Thus, after the analysis end time is reached, one should investigate the model through the following verification approaches: Kinetic/internal energy ratio and Force equilibrium plots.

For a first rough check of the model's behavior, we observe the **Kinetic/internal energy ratio**. We can see in Figure 4.16, that it is close to zero during most of the simulation time, apart from the range between 0 and 0.005 sec, where a steep upward trajectory appears and it reaches a maximum of 0.47204. Of course, the ratio cannot be equal to 0.05 for the whole analysis but it should hold for most of the time, which is the fact in our analysis plot. As such, it seems that for the time being, we receive first good feedback regarding the quasi-static behavior of our model. However, in order to be sure that everything goes well, some more parameters should be also investigated.

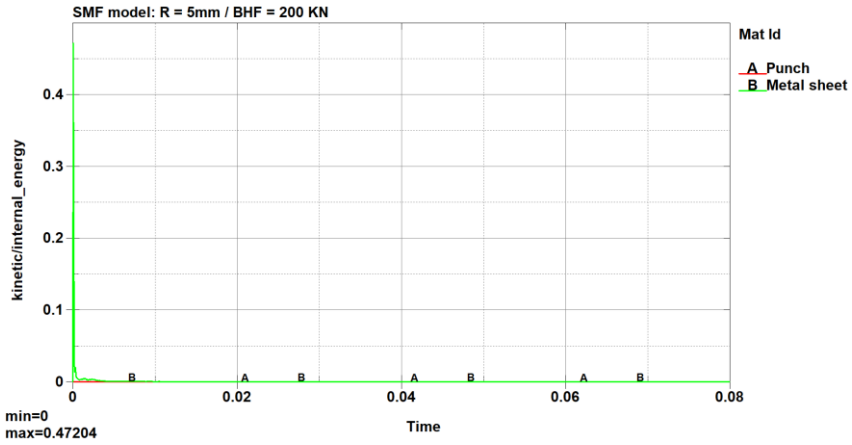

Figure 4.16 Kinetic/internal energy ratio plot

As such, the second parameter which will be studied is the **Force equilibrium** between the punch and the metal workpiece. As mentioned in the previous section, by looking

into that specific plot, we will acquire robust feedback concerning the actual behavior of our model. Even though that method is quite robust to show if our analysis proceeds as planned, sometimes there can still be local effects that don't show up in global force balance. Therefore, after finishing with the initial forces equilibrium plot, the simulation termination time will be doubled to evaluate the elicited results and see if there are any important differences. Obviously since in the first simulation, the tool moves with a velocity of V = 468 mm/s, by doubling the end time the velocity is reduced to V = 231 mm/s.

By starting with the investigation of the punch and reaction forces of the initial simulation with end time of t=0.08 sec, we can see in Figure 4.17 that the difference between them is really small, nearly negligible. By this result, one can understand that almost all of the energy produced from the punch is received from the blank without important loses. Hence, by considering those results one can say that almost certainly no inertial effects are present inside our model. However, we have to verify through our last step (doubling end time), to be sure that everything works peroperly.

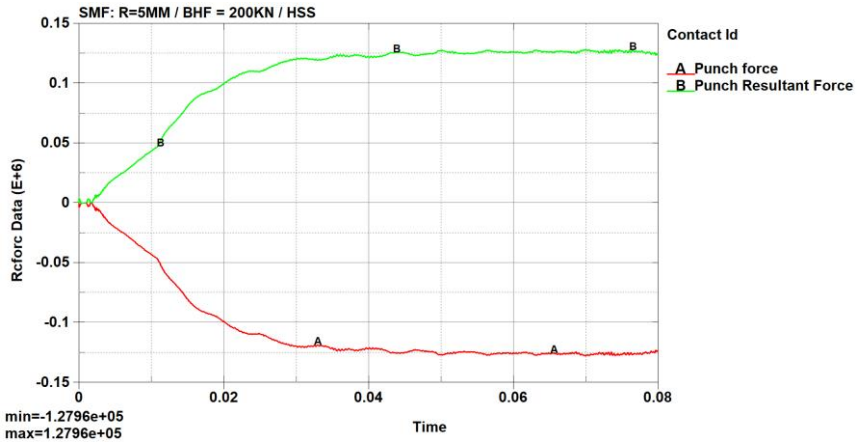

Figure 4.17 Punch and resultant force plot with initial termination time t=0.08sec

By reaching our last step, we will evaluate a second run of the exact same model with the only difference of doubling the end time (t=0.16 sec). So, by observing our new load/reaction forces plot Figure 4.18, we can say that they are pretty much similar. As such, after the second check, we can definitely claim that the model has a fully quasi-static behavior, without the presence of dynamic effects.

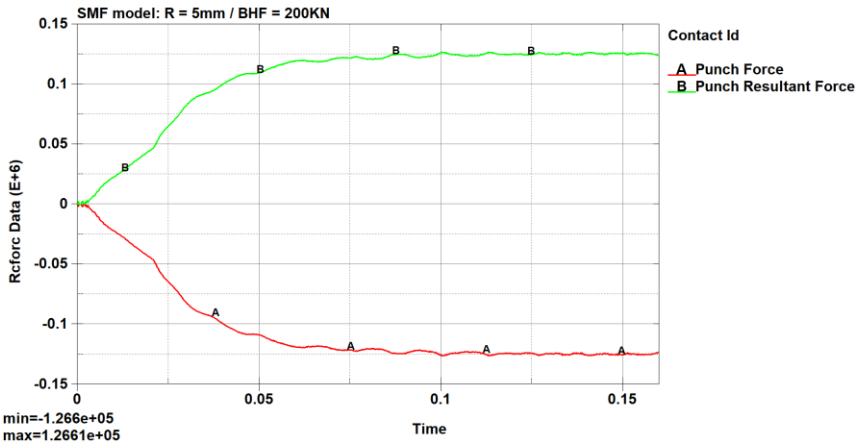

Figure 4.18 Punch and resultant force plot with initial termination time t=0.16sec

Punch Force/Stroke assessment

In order to make a quality estimation of the analysis, the punch forces and the punch displacements of our analysis model can be compared with the corresponding results from publication [23], see Figure 4.19. As it is stated by the author of the research, the values of the punch forces are four times bigger than those from the previous analysis with aluminum. In addition, by looking into the experimental results of [23], the upper border is 101 KN and the lower border is 85 KN (EB 2.01 and EB 2.07 are dismissed). This is the actual experimental force range for that model, using HSS material. The corresponding simulation from the research achieves a force curve laying in between the experimental range with a maximum of ~ 95 KN. Now by taking a look into our analysis plot curve, we can see that it reaches a maximum of 126 KN. In addition, one can observe that during most of the punch movement, the curve is offset by an average of 27 KN. Last but not least, we calculate the error between our plot curve and the upper border of the experimental curves and we extract a value of 23.5 %.

Apart from all those mentioned above, something which is also important to be pointed out is the instability of our initial curve in comparison with the one from [23]. That possibly happens due to some higher frequency oscillations, which are actually generated from the dynamic analysis method. Thus, in order to filter those not useful high frequencies and make the curve smoother, we use a 100Hz Butterworth filter and as such we allow only lower frequencies to come through.

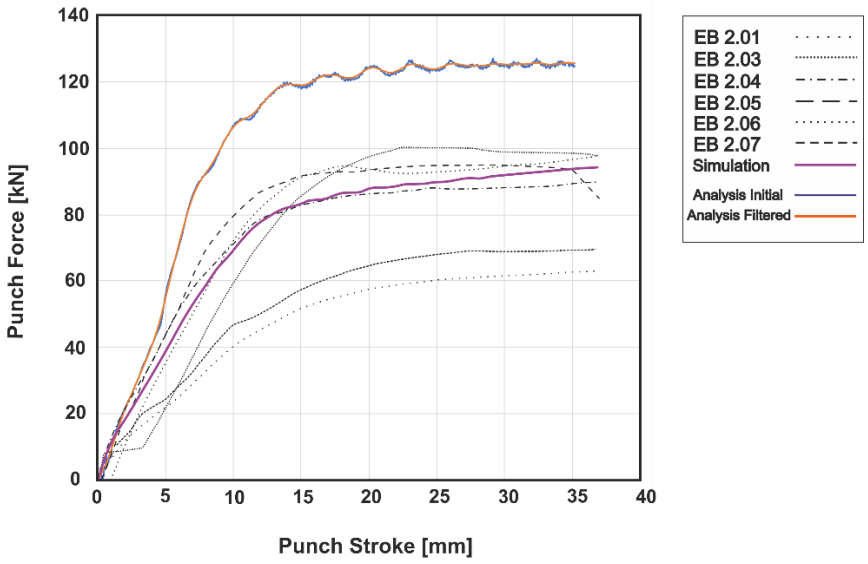

Figure 4.19 HSS, BHF=200KN, Punch Force vs Punch stroke comparison between analysis and [23] results.

Energy ratio and Energy balance

By observing the ratio plot of our simulation, see Figure 4.20, we can easily define that the value is nearly 1 which means that our model satisfies energy conservation and no additional energy is generated. Hence, the simulation runs in a proper way.

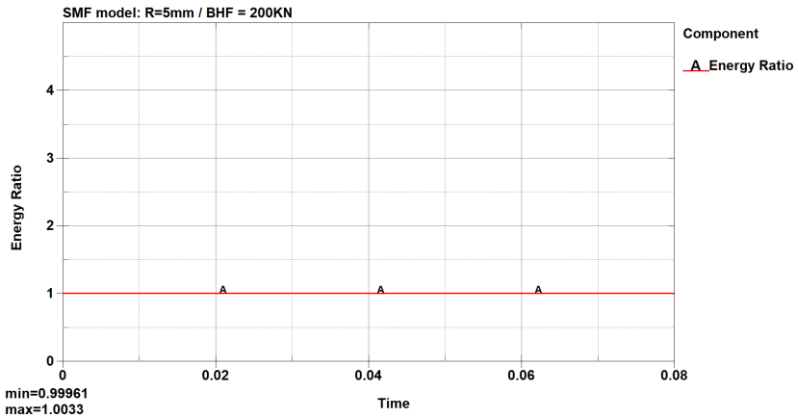

Figure 4.20 Energy ratio plot

Subsequently, we present the general energy plot Figure 4.21, which contains all of the existing energies in our model. Since those curves seem to be smooth without any jumps

as well as the internal energy of the model is much higher than the kinetic energy, it is confirmed once more, that the energy conservation is adequate. [30]

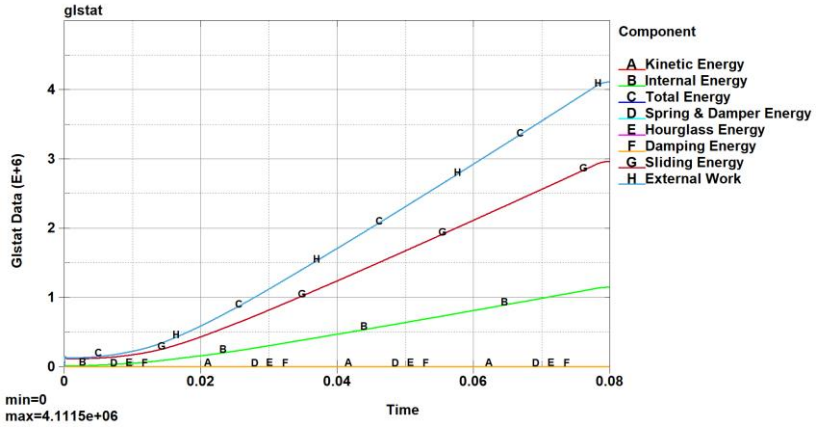

Figure 4.21 Energy summary plot

Forming process results

After confirming that our analysis behavior is quasi-static as well as energy conservation exists, we will continue with the post-processing results display. As mentioned at the start of that chapter, during that simulation the only changes implemented to the model parameters comparing to the previous analysis with AL6111-T4 is the use of HSS material instead of aluminum as well as the increase of BHF which reaches the value of 200KN. Apart from those two, everything else is preserved the same.

Effective (Von-Mises) Stress

To begin with, the first step of results evaluation contains the effective stresses of our model before spring-back. By looking into the values in Figure 4.22, the maximum effective stress of our model is 574.3 MPa. Of course, it is much higher than the corresponding model with aluminum, which seems to be reasonable due to the different and stiffer material but it is lower than the HSS ultimate tensile strength, 615 MPa, so we are in a safe area without being afraid of any necking or even crack failures.

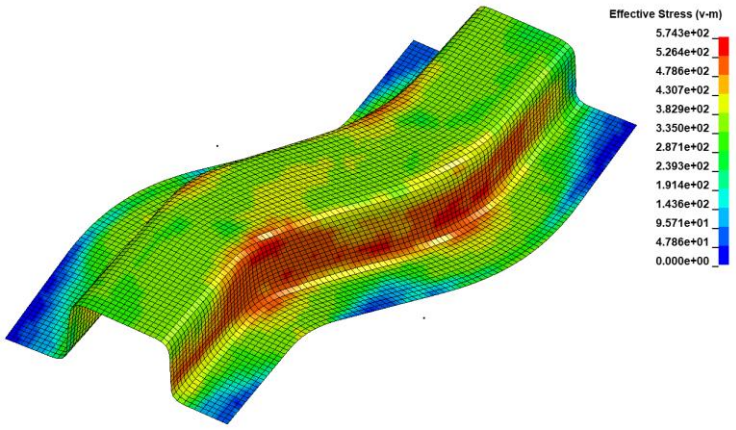

Figure 4.22 HSS, BHF=200KN, Effective von-Misses stresses plot before springback.

The next step is the evaluation of effective stress distribution after springback. As can be seen from the visualization contour Figure 4.23, the stresses of our model reach a value of 420.1 MPa which seems to be logic since the value is lower than the one during the deformation state.

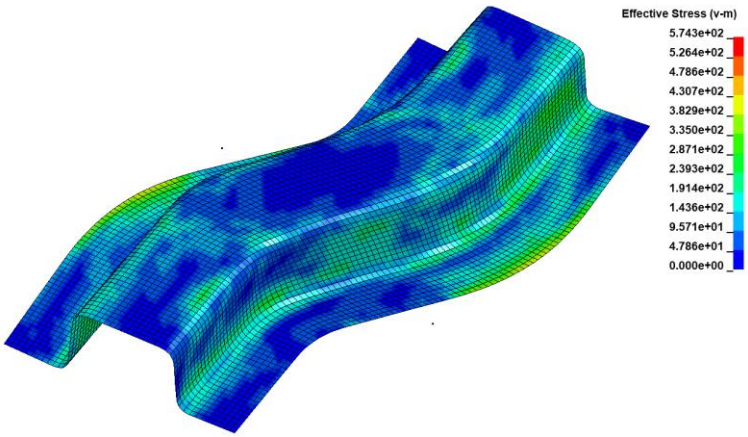

Figure 4.23 HSS, BHF=200KN, Effective von-Misses stresses plot after springback.

Effective Plastic Strain

After evaluating and comparing the stresses of the model, we should also investigate the plastic strain of the workpiece which is also a very important part. By looking into Figure 4.24, one can observe that the maximum plastic strain of the model is 0.255.

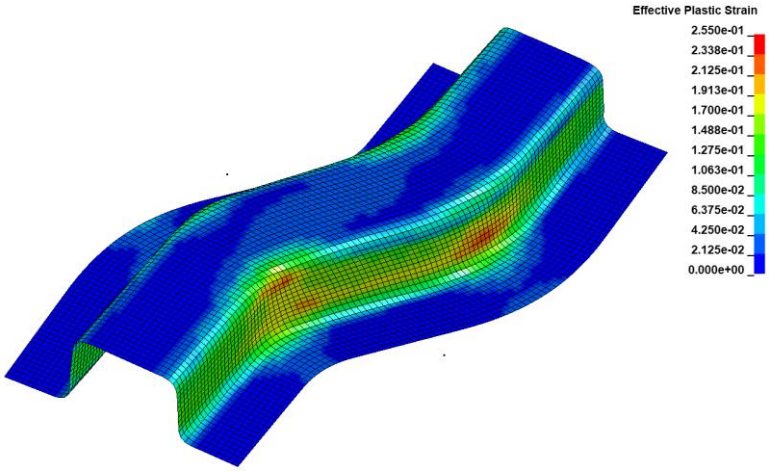

Figure 4.24 HSS, BHF=200KN, Effective plastic strain plot

Material Failures evaluation

To evaluate the simulation concerning the workpiece failures, one should refer to the **thickness reduction plot** as well as the **FLD** and **strain distribution diagram**. Through all of them, a good estimation can be made, concerning the load that the specimen can withstand until cracks appear.

By observing the thickness reduction plot Figure 4.25, we can see that the thickness fluctuates in between a range of -2.96 to 11.79 % of the initial specimen thickness, which is 0.92mm. From a first look, it seems that the material thinning is not that high to provoke cracks on the metal workpiece. Comparing with the previous analysis thinning plot, we can see that the thinning value is increased since larger tensile stresses applied to the specimen whereas thickening decreases, which actually means that wrinkling on the specimen will also be less than the previous analysis. Nevertheless, in order to confirm that those results are valid, we have to also study the FLD plot as well as the strain distribution diagram.

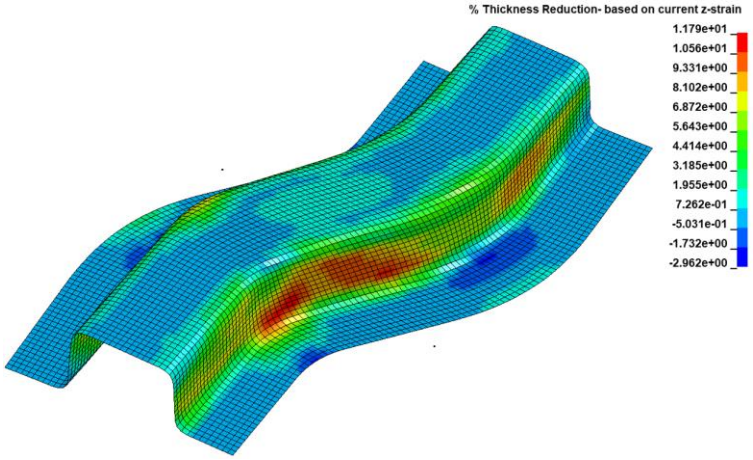

Figure 4.25 HSS, BHF=200KN, Thickness reduction plot

By evaluating the FLD and strain distribution plots in Figure 4.26(a)(b), we can get an idea about the amount of thickness reduction the material can withstand before any cracks occur. From a first glance to the plot, we can see that the results are much better than those from the previous analysis since there are no cracks indications and significantly reduced wrinkles. We can say that the difference between the two analysis results concerning wrinkling reduction is reasonable due to the fact that the blankholder force was increased. Generally, when BHF increases, the wrinkling phenomenon decreases. Apart from that, to further investigate those results, we will take look into the plain geometry of our model Figure 4.27, and see how the real geometry surface looks like. Thus, we can observe also from the plain geometry model, that there are no wrinkles anymore as in the previous analysis. However, in FLD there are again some spots where wrinkling is indicated but in reality, by looking into the plain geometry no wrinkles exist. Given that, through this example, it is confirmed for one more time that the FLD diagram should be used with caution when it comes to wrinkling evaluation.

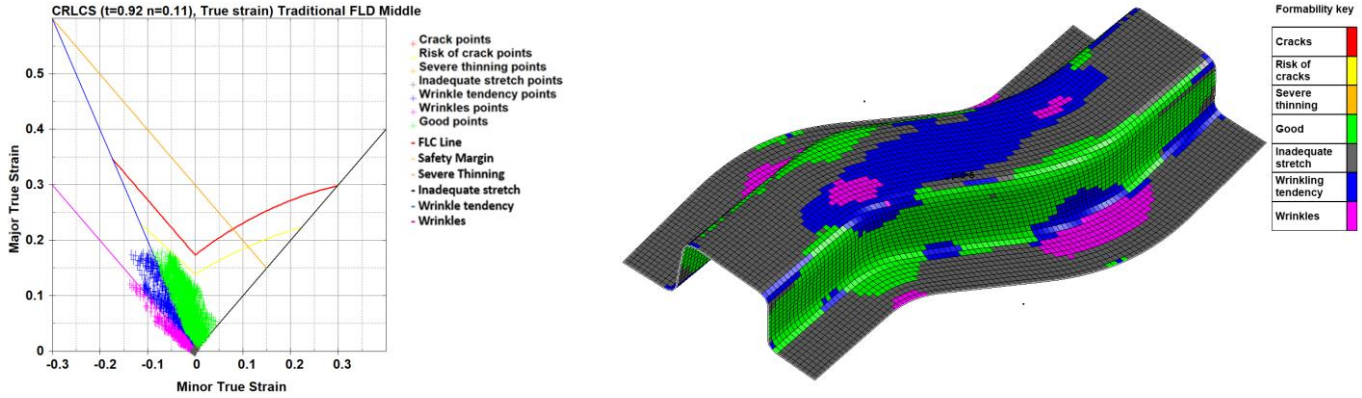

(a) (b)

Figure 4.26 HSS, BHF=200KN, (a) Strain distribution plot in forming simulation, (b) Forming Limit Diagram (FLD) plot

Figure 4.27 HSS, BHF=200KN, Plain geometry without any wrinkling indications

Springback prediction

After the forming process finishes, the next step is springback evaluation. To quantify springback, like in previous analysis, two path lines were considered, J-D and I-E, see in Figure 4.13 (a). One section cut will be applied in each related path. Afterward, along those cuts "before springback" and "after springback" states will be plotted. Last but not least, a comparison between the "after springback" states of specimens will be made, see Figure 4.13 (b), based on the results of our analysis and research [23].

To start with, we will study the first section cut, along the path J-D. The material will remain the same as well as the blankholder force. By looking into Figure 4.28 (a), we can observe that the shape of the specimen changes after springback. Additionally, in Figure 4.28 (b), we make a comparison between the "after springback" states of

specimens, between our analysis and the corresponding values from [23]. As we can see, the displacements have discrepancies of 0.35mm and 0.85mm, for the J and D section side, respectively.

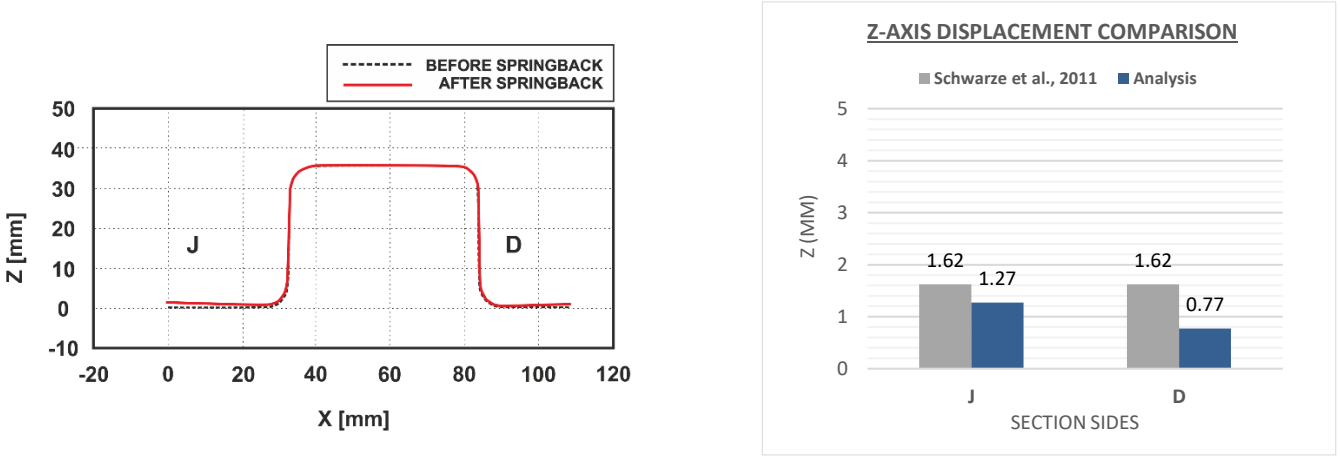

(a) (b)

Figure 4.28 HSS, BHF=200KN, (a) Workpiece deformation before and after springback in section J-D (b) After springback z-axis displacement comparison between **[23]** and Analysis.

Afterward, we will investigate the second section cut along the path I-E. By looking into Figure 4.29 (a), we can observe the elastically unloaded geometry, compared to the initial fully deformed shape. Subsequently, in Figure 4.29 (b), we implement a comparison between the "after springback" states of our analysis and the corresponding one simulation from [23]. As we can see, the springback discrepancies between the two models are 0.19mm and 0.42mm, for the I and E section side respectively. One can observe that the displacements along the I-E path, are smaller compared to those along J-D.

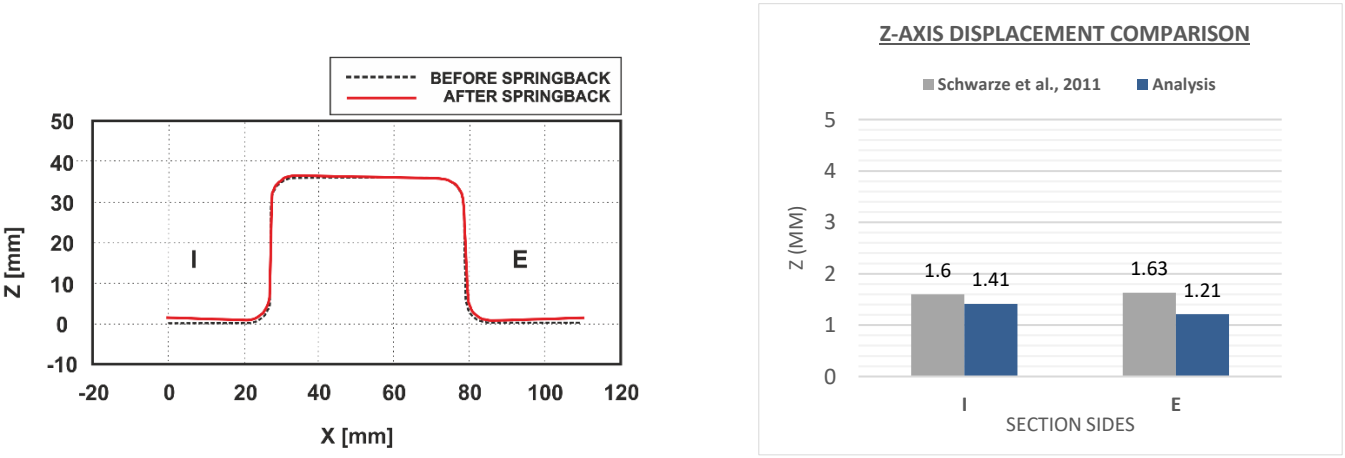

(a) (b)

Figure 4.29 HSS, BHF=200KN, (a) Workpiece deformation before and after springback in section I-E (b) After springback z-axis displacement comparison between **[23]** and Analysis.

Considering the springback results above, one can claim that the overall springback with HSS material and BHF=200KN, is much less than the previous analysis with AL6111-T4 material and BHF=10KN. Therefore, as for the BHF, we can conclude that by increasing the applying force, the springback is reduced and as for the material change, in high strength steel there is less elastic unloading than in aluminum.

4.3 Springback sensitivity evaluation

Elastic unloading in sheet metal forming process is affected by a number of parameters such as die radius, clearance, punch radius, blankholder force, sheet thickness, and material. Hence, in order to observe springback sensitivity, we will modify some of those parameters and in parallel compare the elicited results. The assembly model configuration, as well as some of its parameters (blankholder force, punch radius and die radius), are depicted in Figure 4.30. The springback will be investigated again along J-D and I-E, as in the previous section, see Figure 4.13. During those simulations, in order to measure the actual elastic unloading, the angles $\Theta 1$, $\Theta 2$, $\Theta 3$, $\Theta 4$ will be used, see Figure 4.31. Hence, the amount of springback will be calculated through the difference between the angles before and after the elastic unloading state.

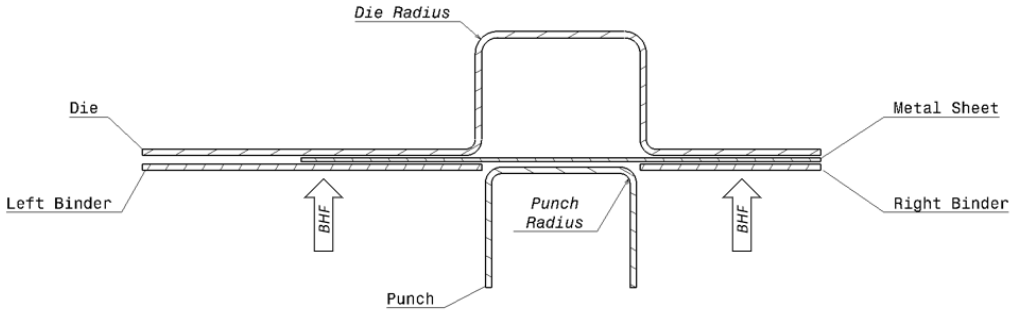

Figure 4.30 S-Rail sheet metal assembly configuration

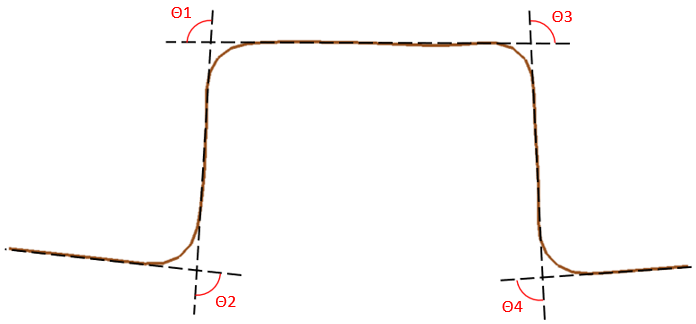

Figure 4.31 Springback measurement angles

Effect of tools radius modification

First of all, we will investigate the elastic unloading sensitivity, during the punch and die radii change. A number of FE simulations will be executed, where each one of them will have a different radius, 4mm, 5mm, and 6mm. During those simulations, the material AL6111-T4 will be utilized, the blankholder force will remain equal to 10KN and the sheet thickness will also not change. As mentioned above in that section we are interested in the quantitative change of springback through the specimen's bending angles. Therefore, it is can be observed that in both sections cuts J-D and I-E, as we can see in Figure 4.32 and Figure 4.33 respectively, by increasing the values of tool radiuses, the springback of the workpiece increases as well. Hence we confirm the already stated in [16], [31] and [32].

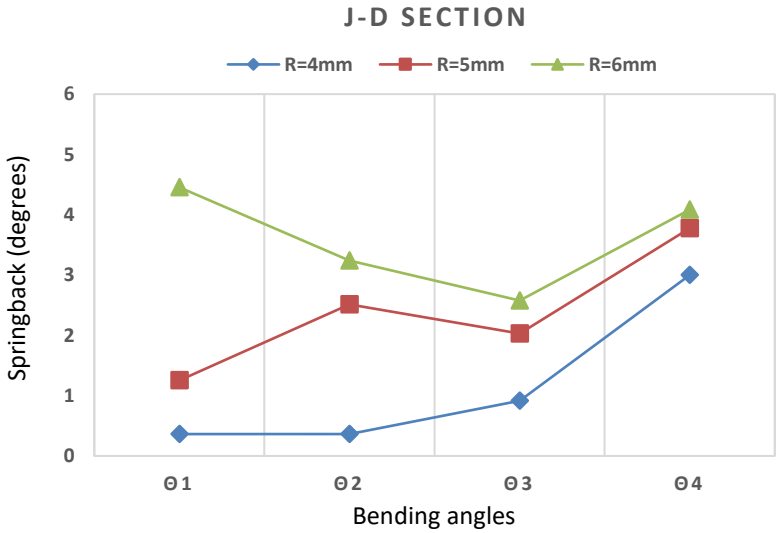

Figure 4.32 AL, BHF=10KN, Comparison of springback between different tools radiuses through J-D section path.

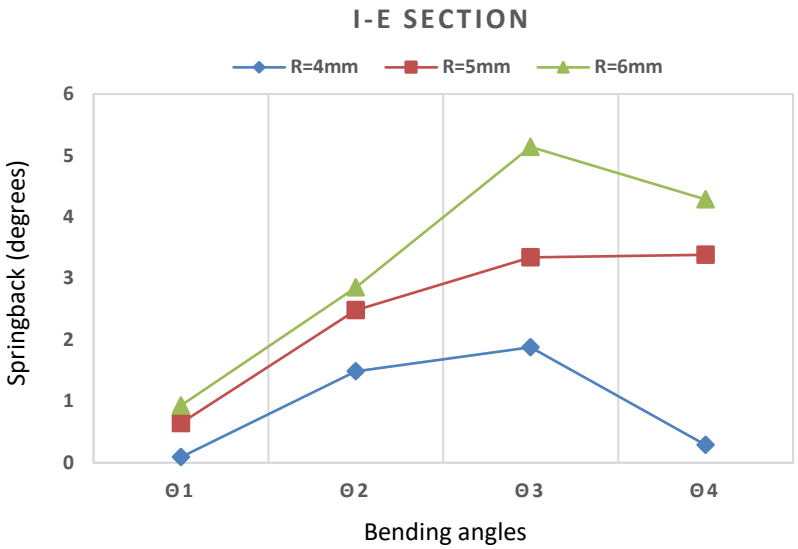

Figure 4.33 AL, BHF=10KN, Comparison of springback between different tools radiuses through the I-E section path.

Effect of BHF modification

In order to observe the effect of blankholder force (BHF) change on elastic material unloading we will run FE simulations with BHF values of 5KN, 10KN and 100KN applied on AL6111-T4 metal workpiece with thickness if 0.92mm. The obtained results are listed in Figure 4.34 and Figure 4.35, so by looking into more detail, we can detect that elastic unloading decreases as the BHF increases in both section paths. Thus, we confirm what is already mentioned in [33], [34] and [35]. This phenomenon is reasonable due to the fact that when applying low BHF, punch induces mostly bending stresses in the material whereas when the blankholder force increases, the stresses induced by the punch become mostly tensile stresses. [32]

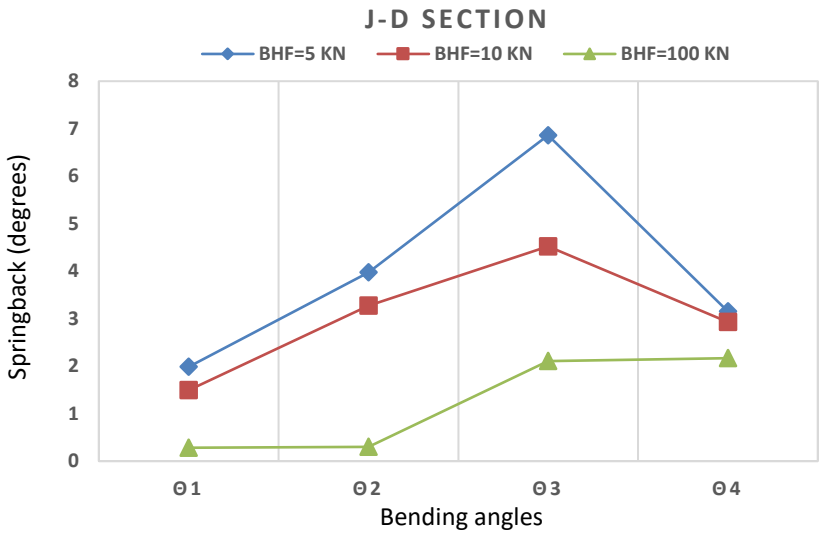

Figure 4.34 AL, Thickness = 0.92mm, Comparison of springback between different blankholder forces through J-D section path

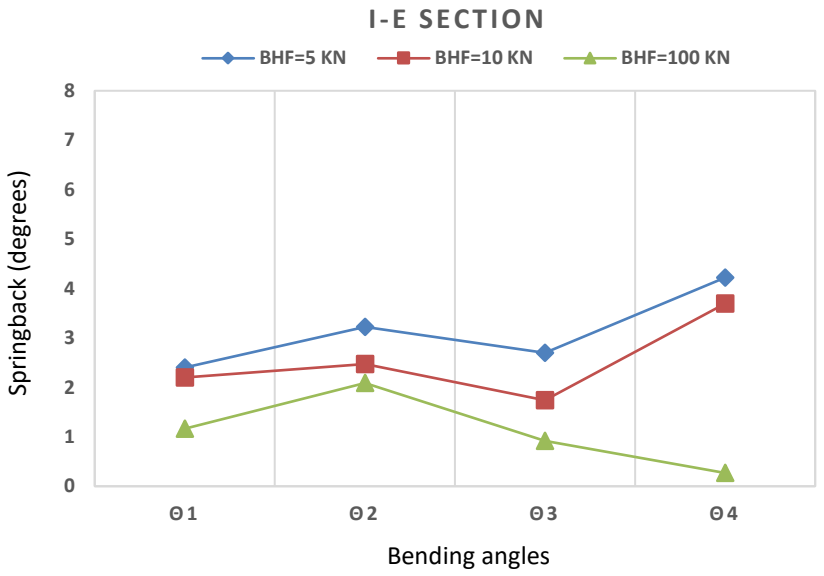

Figure 4.35 AL, Thickness = 0.92mm, Comparison of springback between different blankholder forces through I-E section path

Effect of sheet thickness modification

Apart from the elastic unloading sensitivity in radius and BHF, elastic unloading is also sensitive in sheet thickness alteration. Hence, in order to be able to study that phenomenon, we will run some simulations, using sheet metal specimens of gradually increased

thickness of 0.92mm, 2mm, and 3mm, with a constant BHF equal to 10KN and AL6111-T4 material. By looking into Figure 4.36 and Figure 4.37, we can clearly observe, that while sheet metal thickness increases, elastic unloading is gradually decreased. Such behavior confirms what is already mentioned in [16] and [31].

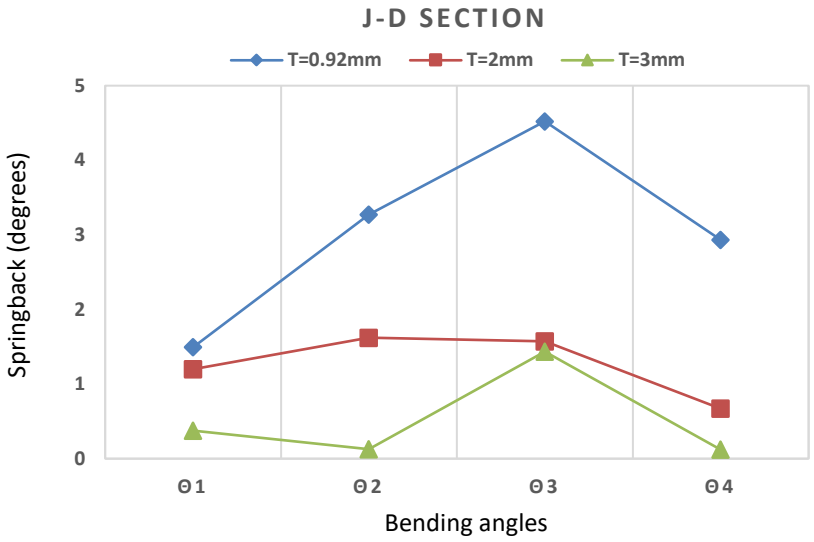

Figure 4.36 AL, BHF=10KN, Comparison of springback between different sheet thicknesses through J-D section path

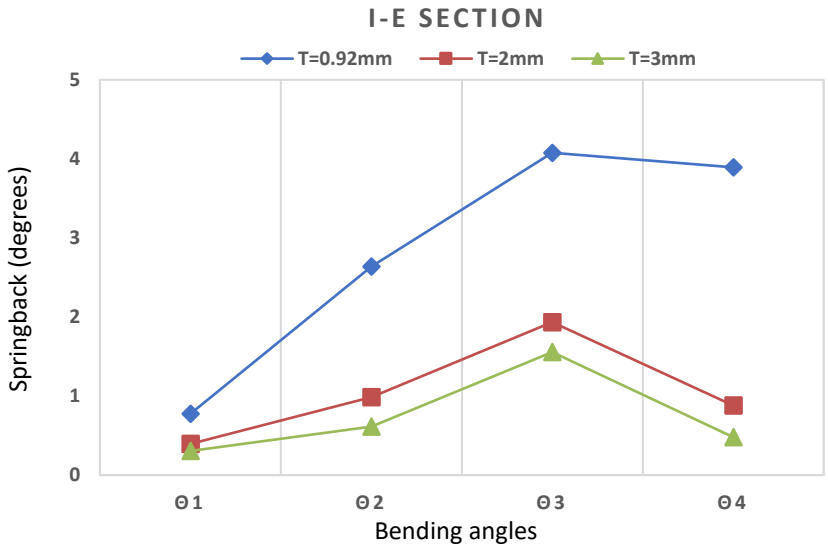

Figure 4.37 AL, BHF=10KN, Comparison of springback between different sheet thicknesses through I-E section path

Chapter 5

Conclusions

During that thesis, a study concerning sheet metal forming deformation, as well as elastic unloading was implemented. Initially, two analysis scenarios were conducted, using different materials, AL6111-T4 and High Strength Steel (HSS) respectively. Those results, elicited from the dynamic deformation as well as from static springback, were compared with some already existing analysis data, from research [23], aiming to calculate the percentage error between those stress - strains values. Subsequently, a study regarding the springback sensitivity on different parameters was also implemented. Given the already mentioned above, the conclusions deriving from the analysis models, are the following:

In the first analysis, using **AL6111-T4** material and **BHF=10KN**, initially by evaluating the forces and energies of the model, we confirm that no inertial effects exist. As for the punch force/punch stroke plots we observe an error of 9.6 %. Subsequently, regarding the deformation state, we notice that the percentage error reaches an average of 15.4 % for stresses and 9.9 % for strains. In addition, as for the specimen's thinning we detect a thickness reduction in a range between -7.65 to 7.75 % which doesn't seem to be alarming. Furthermore, by looking into the Forming Limit Diagram and strains distribution plot results, there are not any ominous indications since no cracks are detected on the blank but only some wrinkling at some specific areas. Concerning the springback

state now, by comparing the values of our analysis with the corresponding ones from [23], firstly we observe in the J-D section cut that is quite small while reaching a maximum of 0.26mm in D side. On the other hand, by looking into the second section cut, I-E, the springback difference increases and it reaches a maximum of 2.02mm on the E side of the specimen.

As for the second analysis, using **HSS** material and **BHF=200KN**, by taking a look into the forces and energies of the model, we can detect that there are no inertial dynamic effects. First of all, as for the punch force/punch stroke plots, we detect an error of 23.5%. Now concerning the deformation state, due to the fact that no results data provided from the [23] for that specific simulation, we cannot calculate any percentage error. However, by evaluating the elicited data, we can notice that there are some reasonable discrepancies, comparing to the first analysis with AL6111-T4, caused due to the change of material as well as the increase of BHF. Furthermore, as for the specimen's thinning, we observe a thickness reduction in a range between -2.96 to 11.79 % which seems sensible due to the BHF increase. Also, by evaluating the Forming Limit Diagram and strains distribution plot, no cracks or risks of cracks are detected again, while wrinkling has been reduced a lot, something that seems to be logical due to the BHF increased value. As for the springback state now, by comparing the values of our analysis and those from [23], in the J-D section cut, we detect a maximum discrepancy of 0.85mm in D side. Now in the I-E cut section, the difference is reduced while it reaches a maximum of 0.42mm in E side.

In general, the percentage error range in most FEA models fluctuates between 0-20%. The actual accepted error level depends on the complexity of the problems as well as on the materials. As stated in [36], the error levels can be split as follows: For simple problems with linear/noble materials, the error should be less than 5% while, in case of complex problems, using non-linear material it can reach values greater than 10%.

In our case, during the first simulation using AL6111-T4 material, we observed that errors reach values of 9.6%, 9.9% and 15.4% at the deformation state. As for the springback state of the model, the discrepancies between the two models reach values of 0.26mm for the D side and 2.02mm for the E side. Considering the fact that our analysis is a complex shaped problem using nonlinear material, we can say that it is within the corresponding error range.

Now as for the second simulation with HSS, we observed an error of 23.5% between the punch force/displacement diagram which is the only value provided during the deformation state. As for the springback state of the model, the differences between the two models reach values of 0.85mm for the D side and 0.42mm for the E side. Regarding this analysis, the force/displacement error is rather big but at the same time, there is a good agreement with small discrepancies between the springback plots. Since we don't have any other values from [23] to compare, we cannot express a more detailed opinion concerning this analysis.

Additionally, a possible reason for those higher than expected error values could be the fact that we used a different element type: shell element instead of a solid-shell element. In order to confirm if this is the actual reason, something could be done in the future, is to simulate that analysis by using solid-shell element type as well as better computational resources.

Regarding the **springback sensitivity** now, since elastic unloading is affected by changing some specific parameters, such as tools radius, blankholder force as well as sheet thickness, we modify them gradually and after that, we compare the elicited results.

To start with, during the first FEM simulations we maintain the BHF equal to 10 KN while in the meantime we modify the punch and die radiuses by giving them different values of 4, 5 and 6 mm. Thus, it is observed that by increasing the tools radii, the angles of the deformed specimen are also increasing in both section cuts (J-D and I-E). So considering the above, we can easily conclude in the fact that the springback increases while the rigid tools radiuses increase, as also stated in [16],[31],[32].

Afterward, we continue in the same philosophy but now we keep the tool radius constant in 5mm and we change the BHF by giving values of 5, 10 and 100KN. Hence, by looking into the elicited plots, we can see that as the BHF increases, the springback gradually decreases. Considering the following literature [33],[34],[35] we can observe that blankholder force is a process that has the biggest influence in elastic unloading intensity. Such behavior occurs, as stated in research [32], due to the fact that mostly bending stresses are induced from punch to the material when BHF is low, while when blankholder force increases, the stresses induced by the punch become mostly tensile.

Finally, in order to investigate the effect that the sheet metal thickness has in springback, the radius is maintained equal to 5mm, the BHF equal to 10KN while we modify the thickness of blank by giving values of 0.92, 2 and 3mm. Thus, as also stated in [16],[31], we observe that the springback is progressively decreasing while the specimen thickness increase.

Bibliography

[1] R. Teti and U. Engel, "Numerical Simulation of Metal Sheet Plastic Deformation Processes through Finite Element Method," p. 420.

[2] S. Jadhav, M. Schoiswohl, and B. Buchmayr, "Applications of Finite Element Simulation in the Development of Advanced Sheet Metal Forming Processes," *BHM Berg- Hüttenmänn. Monatshefte*, vol. 163, no. 3, pp. 109–118, Mar. 2018.

[3] H. S. Valberg, "Applied Metal Forming: Including FEM Analysis," p. 477.

[4] Z. Marciniak, J. L. Duncan, and S. J. Hu, *Mechanics of sheet metal forming*, 2. ed. Oxford: Butterworth-Heinemann, 2002.

[5] T. Altan and A. E. Tekkaya, Eds., *Sheet metal forming: processes and applications*. Materials Park, Oh: ASM International, 2012.

[6] K.-H. Chang, "Introduction to e-Design," in *Product Manufacturing and Cost Estimating Using Cad/Cae*, Elsevier, 2013, pp. 1–38.

[7] F. Lindberg, "Sheet metal forming simulations with FEM," p. 102.

[8] C. D. Joseph, "Experimental measurement and Finite Element simulation of Springback in stamping aluminum alloy sheets for auto-body application," p. 97.

[9] K. B. Nielsen, "Sheet Metal Forming Simulation Using Explicit Finite Element Methods." 1997.

[10] B. B. Prasad, "The theory of continuum and elasto-plastic materials," *Plast. Mater.*, p. 69.

[11] C. Wang, G. Kinzel, and T. Altan, "Mathematical modeling of plane-strain bending of sheet and plate," *J. Mater. Process. Technol.*, vol. 39, no. 3–4, pp. 279–304, Nov. 1993.

[12] R. Sekhara, "Forming Limit Diagram for Sheet Metal Forming: Review."

[13] H. Christophe, "Numerical Simulations of the Single Point Incremental Forming Process," p. 262.

[14] K.-J. Bathe and E. L. Wilson, “Numerical methods in finite element analysis.” 1976.

[15] I. Burchitz, “Springback: improvement of its predictability,” p. 83.

[16] A. H. Alghtani, “Analysis and Optimization of Springback in Sheet Metal Forming,” p. 212.

[17] J. S. Sun, K. H. Lee, and H. P. Lee, “Comparison of implicit and explicit Finite element methods for dynamic problems,” *J. Mater. Process. Technol.*, p. 9, 2000.

[18] G. Noh and K.-J. Bathe, “An explicit time integration scheme for the analysis of wave propagations,” *Comput. Struct.*, vol. 129, pp. 178–193, Dec. 2013.

[19] A. M. Prior, “Applications of implicit and explicit finite element techniques to metal forming,” *J. Mater. Process. Technol.*, vol. 45, no. 1–4, pp. 649–656, Sep. 1994.

[20] R. H. Wagoner, J. F. Wang, and M. Li, “Springback,” 27-Feb-2006. [Online]. Available: http://li.mit.edu/Stuff/RHW/Upload/49.pdf. [Accessed: 14-Sep-2019].

[21] “How contact works,” *Welcome to the LS-DYNA support site*. [Online]. Available: https://www.dynasupport.com/tutorial/contact-modeling-in-ls-dyna/how-contact-works. [Accessed: 14-Sep-2019].

[22] J. Jakumeit, M. Herdy, and M. Nitsche, “Parameter optimization of the sheet metal forming process using an iterative parallel Kriging algorithm,” *Struct. Multidiscip. Optim.*, vol. 29, no. 6, pp. 498–507, Jun. 2005.

[23] M. Schwarze, I. N. Vladimirov, and S. Reese, “Sheet metal forming and springback simulation by means of a new reduced integration solid-shell finite element technology,” *Comput. Methods Appl. Mech. Eng.*, vol. 200, no. 5–8, pp. 454–476, Jan. 2011.

[24] M. Bäker, “How to get meaningful and correct results from your finite element model,” *ArXiv181105753 Cs*, Nov. 2018.

[25] “What is the commonly used contact type in stamping analysis?,” *Welcome to the LS-DYNA support site*. [Online]. Available: https://www.dynasupport.com/faq/metal-forming/what-is-the-commonly-used-contact-type-in-stamping. [Accessed: 09-Sep-2019].

[26] B. N. Maker and X. Zhu, “Input Parameters for Metal Forming Simulation using LS-DYNA,” p. 10.

[27] B. N. Maker and X. Zhu, “Input Parameters for Springback Simulation using LS-DYNA,” p. 11.

[28] “LS-DYNA-Keyword user’s manual, Volume I.” LSTC, May-2007.

[29] B. N. Maker, “User’s Guide to Static Springback Simulation using LS DYNA.” Livermore Software Technology Corporation, Aug-1998.

[30] “Energy data,” *Welcome to the LS-DYNA support site*. [Online]. Available: https://www.dynasupport.com/tutorial/ls-dyna-users-guide/energy-data. [Accessed: 02-Sep-2019].

[31] S. Gawade and V. Nandedkar, “Investigation of springback in U shape bending with holes in component,” *Ind. Eng. J.*, vol. 11, no. 9, Sep. 2018.

[32] L. Papeleux and J.-P. Ponthot, “Finite element simulation of springback in sheet metal forming,” *J. Mater. Process. Technol.*, p. 7, 2002.

[33] J. Choi, J. Lee, G. Bae, F. Barlat, and M.-G. Lee, “Evaluation of Springback for DP980 S Rail Using Anisotropic Hardening Models,” *JOM*, vol. 68, no. 7, pp. 1850–1857, Jul. 2016.

[34] B. Chirita and G. Brabie, “Control of Springback Intensity in U-Bending through variation of Blankholder force,” p. 5.

[35] K. Jiang, Y. Hou, J. Lin, and J. Min, “A springback energy based method of springback prediction for complex automotive parts,” *IOP Conf. Ser. Mater. Sci. Eng.*, vol. 418, p. 012104, Sep. 2018.

[36] “In finite element analysis verification and validation with field tests, universally what is the expected percentage FEA should meet?,” *ResearchGate*. [Online]. Available: https://www.researchgate.net/post/In_finite_element_analysis_verification_and_validation_with_field_tests_universally_what_is_the_expected_percentage_FEA_should_meet. [Accessed: 01-Oct-2019].